NTNU

Norwegian University of
Science and Technology

Skin effects and UV dosimetry of climate therapy in patients with psoriasis

Veronika Bartosova

Master of Science in Electronics
Submission date: June 2010
Supervisor: Lise Lyngsnes Randeberg, IET

Norwegian University of Science and Technology
Department of Electronics and Telecommunications

Problem Description

Controlled sun exposure through climate therapy is an effective treatment for psoriasis. Even though this treatment gives the patients relief from their discomforting symptoms, it has some potentially harmful side effects such as sunburn (erythema) and thereby potential risk of skin cancer. It is therefore desirable to optimize the treatment effect and minimize the side effects during climate therapy. Such optimization can for example be based on evaluating the skin changes during treatment, through optical spectroscopy of the skin and in relation to acquired UV dose monitored by personal dosimeters. The main aim of this project is to propose an inverse model to be used with an existing diffuse skin model to extract the properties of the skin of the patients undergoing climate therapy.

The project solution should include:

Thorough description of the background for the project. Including description of skin, psoriasis and their interactions with sun exposure and a description of the principles and physics of the skin diffusion model that has been used.

A description of a proposed inverse model and parameters used to numerically evaluate the skin properties, together with theoretical preparation for the practical future measurements including UV dosimeters and data handling.

Results of testing of the inverse model performance on normal skin spectra with values of the skin specifications. Results of the inverse model ability to fit the diffuse skin model simulated spectra to the measured samples of psoriatic skin.

Discussion of the model performance in both cases.

Assignment given: 18. January 2010
Supervisor: Lise Lyngsnes Randeberg, IET

Skin effects and UV dosimetry of climate therapy in patients with psoriasis

Veronika Bartošová

Supervisors: Lise Lyngsnes Randeberg (NTNU)
Lill Tove Norvang Nilsen (NRPA)

Master Thesis

Trondheim, June 2010

Acknowledgement

This thesis was realized at the Norwegian University of Science and Technology (NTNU) in The Faculty of Information Technology, Mathematics, and Electrical Engineering at The Department of Electronics and Telecommunications in cooperation with the Norwegian Radiation Protection Authority (NRPA).

I would especially like to thank to my supervisor at NTNU Lise Lyngsnes Randeberg for her inspiring, positive and organized guidance, to Lill Tove Norvang Nilsen from NRPA for her comments, support and contagious enthusiasm for the topic. I would also like to thank dermatologist Dr. Anne-Lene Krogstad and the personnel at the Norwegian Health Centre at Valle Marina, Gran Canaria, for constructive input to problems to be addressed. I also very much appreciate the contribution of Tore Landsem for taking part in the skin measurements.

In particular I want to express thanks to my parents for inspiring and sharing my dreams and goals and especially to Alex for his comprehensive tireless support and help.

Abstract

Sun exposure and climate therapy is an effective treatment for psoriasis. However, even though this treatment gives the patients relief from their discomforting symptoms, it has some potentially dangerous side effects such as an increased risk of skin cancer and premature skin aging.

A prospective field study plans to follow the patients undergoing the climate therapy. During this study the UV dose to each patient will be monitored by personal dosimeters worn by the patients. Furthermore the patients' skin spectra acquired by the means of optical spectroscopy will be obtained daily. Both psoriatic skin a unaffected skin will be observed. These data will be used to assess the skin changes which take place during the psoriasis treatment.

This project is focused on developing an automatic algorithm for handling bulk spectrometric measurements data and to propose ways of numerically evaluating the skin spectra. These numerical values will be later used to compare the daily patients' spectra and monitor progress of the treatment.

An inverse model based on a lookup table and successive iteration was proposed in this project. The model matches the diffuse skin reflectance spectra modeled with a diffuse skin model with the measured patients skin spectra. The measured skin spectra are then defined by the diffuse skin model input parameters which were found by the inverse model. These parameters are oxygenation, blood volume and melanin absorption coefficient. Additionally four indexes were proposed to supplement the parameters found by the inverse model, namely the erythema index, melanin index, hemoglobin index and oxygenation index. Measurements of several skin spectra including psoriatic plaques spectra were carried out and used to test the inverse fitting model performance.

The proposed model proved to match the measured spectra in an acceptable form employable for distinguishing between different measured spectra. The highest deviation is at the ends of the spectra due to the use of a constant value of scattering coefficient and additional parameters not directly relevant to sun exposure, hence not considered by the model. The proposed parameters together with the indexes proved to be a viable means of evaluating the healing in the psoriatic plaques as well as determining the changes caused by the sun in normal skin.

Contents

List of Figures

Part I

Introduction and Theoretical Background

1

Introduction

This master thesis was elaborated in continuation of the earlier specialization project [8] dedicated to the objective consideration of the risks connected to the treatment of psoriasis in the form of climate therapy.

Psoriasis is an incurable skin disease accompanied by symptoms which in severe cases can seriously affect the patients' quality of life. Psoriasis symptoms are hard to treat since no treatment is universal for all patients, and it has significant economical impact on the healthcare system. Climate therapy is one of the least invasive methods available to deal with psoriasis symptoms. Norwegian patients are sent for three weeks to a climate therapy center on The Canary Islands. At this center the patients follow a prescribed schedule which consists of sun exposure periods, an education program with different psoriasis related lectures, exercise routines, healthy diet and socialization programs.

In the earlier specialization project [8] the different factors influencing the UV dose delivered to the patient were considered and a sun-bathing schedule was formed in the interests of minimizing the erythema and thereby potentially connected cancer and skin aging risks and maximizing the beneficial therapeutic effects of UV exposure.

This current thesis was originally intended to complement the aforementioned project with a new approach to the topic; namely with the use of a diffusion model for photon transport in skin (diffuse skin model developed by Svaasand et al. for example [9, 10]) and skin spectroscopy to describe and asses the changes that take place during relatively intensive and organized sun exposure therapy. These goals were to be based on a rich collection of data acquired on site at the climate therapy center, where spectroscopic measurements would take place. Unfortunately these measurements could not take place due to travel complications caused by sudden activity of the Icelandic volcano Eyjafjallajökull. The next term for these measurements was set in October and hence they are not available for this thesis. For these reasons the focus shifted to a much more theoretical level and is understood as theoretical and methodological preparation for the measurements which will take place in the future.

This thesis now aims to develop an inverse model to fit and evaluate the measured spectra with the use of an existing skin diffuse model and its input parameters. It also attempts to find a set of parameters which will be used to define the different and changing skin properties of the patients undergoing the climate therapy and will supplement the diffuse skin model input parameters. Both sets of parameters will take into account the oxygenation, melanin and hemoglobin content of the measured skin, in addition erythema index will be calculated for the measured spectra. The developed inverse model was tested on real spectra of both normal and psoriatic skin.

The reason for solving this task is the large volume of data to be handled, which calls

for an automated evaluation of the measurements. For the climate therapy patients' skin measurements, about 20 patients are expected to take part in the study. These patients will be measured twice a day, in the morning and in the evening, for the period of 21 days. This estimated course of the experiment would then require the evaluation of approximately 840 spectra, which would be very demanding, inefficient hence potentially inaccurate if done manually. These issues were previously explored by Wim Verkruysse et al. in [11].

Furthermore this project deals with the preparation of the UV dosimeter measurements, including the issue of handling the somewhat flimsy available dosimeters as well as with the task of handling the complete patients' data.

1.1 Structure of the Project

This project is divided into three parts. The first part *The Introduction and Theoretical Background* gives the necessary theoretical information which form the basis of this project. These include an overview of skin anatomy, a description skin optical properties description and the basics of skin UV radiation interactions. Psoriasis and its mechanisms are introduced, together with brief description of its possible treatments which involve the use of UV radiation. In this part the background mathematical theory on which the used diffuse skin model is based is introduced together with the principle of skin spectroscopy.

The second part, *The Methods and Instrumentation* deals with descriptions of the mechanisms behind the diffuse skin model and the realized inverse model together with their variable parameters, it also summarizes the proposed skin properties evaluation. This part also contains chapter describing the spectrometer setup used, the preparation of the UV dosimeters and patients data handling.

The third part includes the chapters of results, discussion and conclusion where the results of the inverse model and skin parameters are presented and evaluated.

2

Theoretical Background

2.1 Skin Structure

Human skin is very inhomogeneous tissue; it is differentiated in various ways depending on the body site and it contains several specialized cell types (sweat glands, hair follicles, etc.). The outer layer of the skin is *the epidermis*, a stratified layer of squamous keratinocytes. The inner layer is *the dermis* and consists mainly of collagen and elastic fibers. Under the skin we can find subcutaneous tissue formed by dense connective tissue fibers [12, 13]. The skin structure is illustrated on figure 2.1.

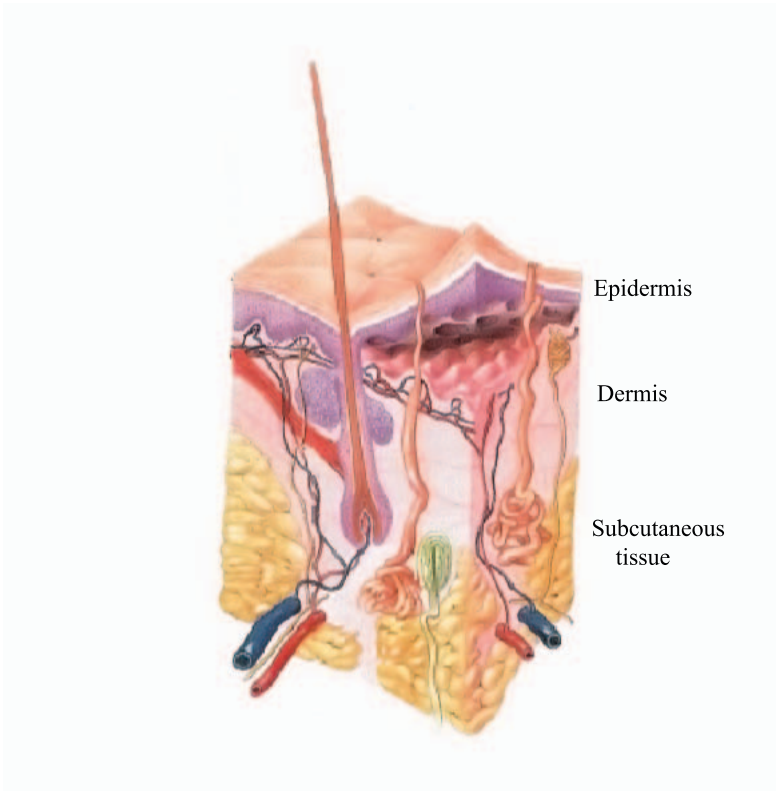

FIGURE 2.1: Skin structure [1]

2.1.1 Epidermis

Depending on its location on the body, the thickness of epidermis is about 50 to 150 μm [12]. On the soles of the feet and the palms of the hand the epidermis is much thicker and it forms the unique pattern of papillary ridges.

Epidermis itself consists of four layers. In the lowest cellular layer called *stratum germinale* (which consists of basal and prickle cell layers) the cells divide continuously. After

division the newly formed cell migrates to the surface of the skin. On the way they form granules (*stratum granulosum*) or lose their nuclei to form *stratum lucidum* in the palms of the hand and soles of the feet. When the cells reach the surface of the skin (*the horny layer*) they become flattened in a protective layer over the other living cells and eventually fall off as keratinous scales.

There are other specialized cells to be found within epidermis; Merkel cells being secondary mechanosensory cells (in fingertips), Langerhans cells taking part in the specific immune system and melanocytes which are pigment producing cells of a great interest from spectroscopic point of view [12, 13].

2.1.1.1 Keratin and Keratinocytes

Electron microscopical examination of cells from all tissues reveals that they contain a complex, heterogenous, intracytoplasmic system of filaments. Numerous classes of intermediate filaments can be recognized in different cell types; keratin are those found in epithelial cells. In cultured epidermal cells, keratins account for up to 30% of the cellular protein, while in stratum corneum, keratin accounts for up to 85% of the cellular protein [14].

The type of keratin differs in different tissues such as for keratinized epidermis, hyperproliferative epidermis of palms and soles and simple epithelium of the epidermal glands. Keratin is the main structural protein of the epidermis.

The keratinocytes in the basal layer synthesize keratin filaments which aggregate into bundles. Then in the cells of the stratum corneum, these bundles of keratin filaments form a complex intracellular network embedded in a protein matrix. Epidermal keratinization results in the production of a barrier which is relatively impermeable to substances passing in or out of the body [14].

2.1.2 Dermis

Dermis lies under the epidermis and forms a much thicker layer, around 1 to 4 mm. It mainly consists of connective tissue cells (collagen and elastic fibers) and gives the skin support and elasticity. It also contains nerve cells, blood vessels and lymphatics, all of which are situated in the outer dermal layer *papillary dermis*. The innermost layer *stratum reticulare* is formed by fatty tissue and elastic fibers, and works as a shock absorber and an insulator [12, 13].

2.1.3 Skin Pigments and Chromophores

Skin color is given by the interaction of incident light with the pigments present in the skin and with the blood contained in the dermal vessels, these represent the absorption part of the skin – light interaction. The most important skin pigments are melanins, hemoglobin, bilirubin and carotenoids. Scattering of collagen fibers and other cellular structures also influences the skin color appearance [15].

2.1.3.1 Melanins

Melanocytes are large cells with long dendrites responsible for the production of melanin, a pigment that gives the skin and hair their color. Melanocytes are located in the *stratum basale* of the epidermis. Melanin pigment is a polymer made of tyrosinase amino acids [12]; it occurs in colors from yellow to reddish-brown and black. Its majority is located in the epidermis *stratum germinale* basal layer and within the hair follicles. The skin color caused by melanin is the result of the melanin synthesis and its distribution to surrounding keratinocytes. Melanocytes form only approximately 10% of all epidermal cells. They interact with the neighboring keratinocytes through their dendrites and this way also transfer the melanosomes [13]. Melanosomes are special melanin-containing organelles about 1 μm in diameter. The melanosome transfer is critical for normal skin pigmentation. Melanocytes with their melanin production are indispensable in the photo-protection against UV radiation [16, 17].

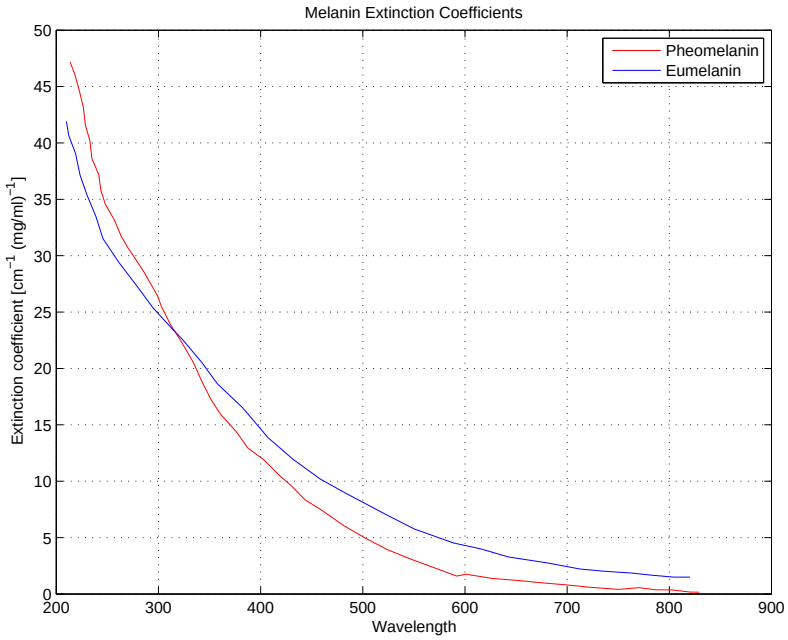

FIGURE 2.2: The eumelanin and pheomelanin extinction coefficients [2]

The variety of human skin colors is caused by several factors. These factors include the rate of synthesis of melanin by melanocytes, the relative amounts of eumelanin (the brown-black pigment) to pheomelanin (the red-yellow pigment), the size of melanosomes and the transfer characteristics to the surrounding keratinocytes. In dark skin, melanosomes are larger and more frequent; these are then transferred one by one to the keratinocytes. Their content of eumelanin is higher over pheomelanin than in light skin and the keratinocytes retain the eumelanin longer [12]. In light skin the melanosomes are transferred in clusters [16, 13]. Keratinocytes are able to interact with melanocytes with production of biochemical mediators. Melanocytes, through the production of melanin, form protection of the skin against damage caused by inflamation or UV radiation exposure; it is suggested that

increased melanin production is part of stress response and can be induced by DNA damage [18]. Skin pigmentation is the result of a sophisticated process regulated by several factors located on site in the skin or generated in distant tissue and transported via blood circulation.

Melanin absorption ranges from the ultra-violet into the near infrared parts of the spectrum, its absorption decreases with increasing wavelength (proportional to $\lambda^{-3.46}$) and is the strongest in the UV region [19], its extinction coefficients can be seen on figure 2.2.

The extinction coefficient is defined as the probability of photon interaction with the medium per unit path length. Extinction itself includes absorption and scattering.

2.1.3.2 Carotenoids

Carotenoid absorbers are red pigments, mostly represented by betacarotene. Carotene is a yellow to orange pigment found in certain plant products such as carrots. It is soluble in lipids and it tends to accumulate in subcutaneous fatty tissue and stratum corneum after consumption of fruits and vegetables. Its color is most obvious in the palms and soles, where the stratum corneum is the thickest and most intense when large amounts of carotene rich food are eaten. However the yellow-ish hue of the skin of Asian people is due to variations in melanin as well as to carotene [13]. Betacarotene absorption peak is found at 450 nm and 480 nm [20] as illustrated on figure 2.3.

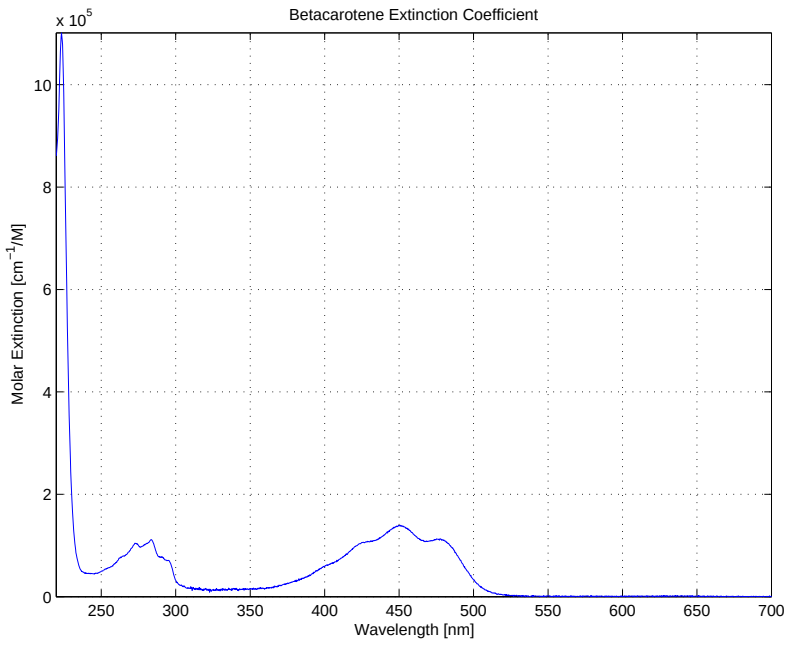

FIGURE 2.3: Betacaroten extinction coefficient [3].

2.1.3.3 Hemoglobin

Hemoglobin is a found in erythrocytes (the red blood cells), it is a molecule that binds to and transports gases (oxygen and carbon dioxide). It is made of the protein globin bound to the red heme pigment. Globin is made of polypeptide chains, each bound to a circular heme group [13]. Each heme bears in its middle an atom of iron. Each iron atom can combine reversibly with one oxygen molecule, and each hemoglobin molecule can transport four oxygen atoms. Each red blood cell contains about 250 million hemoglobin molecules. Erythrocytes work as a protection of hemoglobin so it doesn't break into fragments which would leak out of the vessels through porous capillary membranes. In the lungs, oxygen diffuses into the blood and into the erythrocytes, where it binds to hemoglobin. This form of hemoglobin is called oxyhemoglobin, it assumes a three dimensional shape and appears bright red. In tissues the oxygen detaches and diffuses into the tissue leaving the hemoglobin in deoxyhemoglobin form which is dark red. About 20% of carbon dioxide in the blood stream binds to hemoglobin amino acids and this is called carbaminohemoglobin and occurs more readily in reduced state (without oxygen attached). Carbaminohemoglobin has dark red-ish blue color [21].

From the skin optical properties point of view, it is significant that different forms of hemoglobin have different absorption peaks. Deoxyhemoglobin absorption maxima are at 550 nm and 760 nm. Oxyhemoglobin maxima are at 548 nm and 576 nm [5]. Methemoglobin, which forms when hemoglobin is exposed to oxidative stress, heating or UVB exposure has absorption peaks located at 404 nm, 508 nm and 635 nm.

2.1.3.4 Urocanic Acid

Urocanic acid is an epidermal chromophore, which shows immunomodulatory behavior. Urocanic acid exists as trans-isomer and cis-isomer shown in 2.4, in the uppermost layer of the skin (stratum corneum) [22].

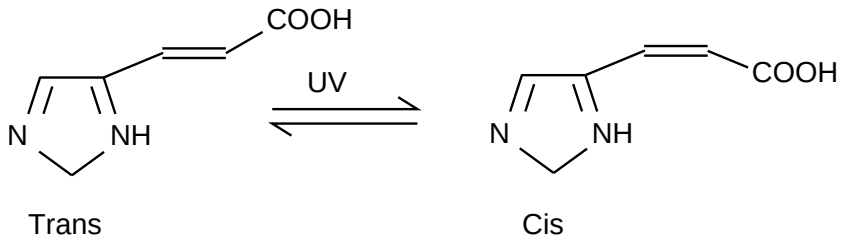

FIGURE 2.4: Trans- and Cis-isomers of the urocanic acid molecule which can be flipped with UV - radiation.

The trans-isomer of the urocanic acid is formed as the cells of the epidermis become metabolically inactive. During this process, proteins and membranes degrade, histidine aminoacid is released, and histidase (histidine ammonia lyase) catalyzes the deamination of histidine to form trans urocanic acid. This accumulates in the epidermis until removal by either the monthly skin renewal cycle or through sweat. With UV light ab-

sorption the trans urocanic acid izomerizes to cis form. Early researches [22] proposed that urocanic acid was a natural sunscreen absorbing UV-B in the stratum corneum as demonstrated on its absorption spectra on figure 2.5, but later it was found out that its cis-form amongst others also affects natural killer cell (immune system white blood cells) activity. Cis urocanic acid is now assumed to act as a mediator for UV-induced immunosuppression [22, 23]. This is believed to be one of the possible immuno suppression effects of phototherapy which is used also as one of the psoriasis treatment methods [24, 25].

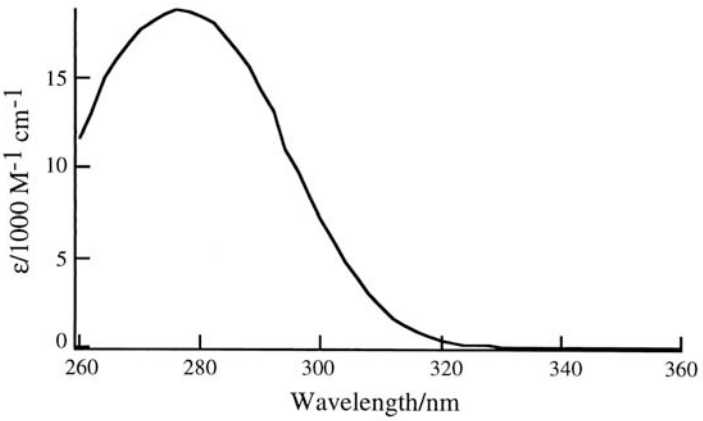

FIGURE 2.5: The absorption spectrum of naturally occurring trans-urocanic acid [4]

2.2 Skin Changes Caused by UV Exposure

2.2.1 Skin Darkening

Exposure to the sun causes immediate skin darkening due to photo-oxidation of pre-existing melanin and reorganization of dendrites as preparation for melanosome transfer. This occurs within minutes after sun exposure and is attributed mainly to UVA radiation. Delayed tanning response is then caused by increased production and transfer of melanin to keratinocytes, and is caused by UVA and UVB.

There are several skin types divided according to the response of the skin to sunlight, and to its erythema reaction. Table 2.1 gives the Fitzpatrick classification of the skin phototypes [26]. Excessive sun exposure of the skin can also lead to sunburn as described in section 2.5.1.

Photo-type	**Sunburn and Tanning**	**Immediate Tanning**	**Delayed tanning**	**Unexposed skin**	**UVA MED**	**UVB MED**
I	Burns easily, never tans	None	None	Ivory White	20–35	15–30
II	Burns easily, tans minimally	Weak	Minimal/ weak	White	30–45	25–40
III	Burns moderately, tans moderately	Definite	Low	White	40–55	30–50
IV	Burns minimally, tans moderately	Moderate	Moderate	Beige-Olive	50–80	40–60
V	Rarely burns, tans profusely	Intense (brown)	Strong	Moderate brown	70–100	60–90
VI	Never burns, tans profusely	Intense (dark brown)	Strong	Dark brown/ black	100	90–150

TABLE 2.1: Fitzpatrick's Skin Phototypes [26], The unit MED is in (mJ/cm^2) further described in section 2.6.

2.2.1.1 Skin Cancer

There are several types of skin cancer. Skin cancer that forms in melanocytes is called melanoma (CCM cutaneous malignant melanoma). Skin cancer that forms in the lower part of the epidermis is the basal cell carcinoma (BCC). Skin cancer that forms in squamous cells (the flat cells that form the surface of the skin) is the squamous cell carcinoma (SCC) [27]. The incidence rate of each of the cancer types is higher in fairer skinned, sun-sensitive rather than darker skinned, less sun-sensitive people. The risk is increased with increasing level of ambient solar radiation and the highest rate of occurrence is on the most sun exposed parts of the body. The different types are associated in individuals with life – long and occupational exposure for SCC and non-occupational or recreational sun exposure with a history of sunburn and presence of benign sun damage in the skin for melanoma and BCC [28].

2.2.2 Vitamin D Production

Skin exposure to the UVB part of the solar spectra is also responsible for the production of vitamin D. Photons with wavelengths of 290 to 315 nm penetrate into the skin where they interact with cholesterol structures to form the precursor of vitamin D, previtamin D3. Previtamin D3 can also further absorb ultraviolet radiation and form photoisomers

that later take part in calcium metabolism. When previtamin D3 is exposed to body temperature it can spontaneously rearrange over approximately one day to form vitamin D3 [29].

2.2.3 Photoaging

Most of the visible signs of skin aging such as wrinkles, leathered appearance, sagging and overall loss of elasticity are believed to result from chronic life-long exposure to ultraviolet radiation, and hence UV-induced photodamage [4, 30]. Increased exposure of the skin to UV radiation increases the risk of photooxidative damage leading to long term effects of photoaging.

Unlike chronologically aged skin that results from a general atrophy and a gradual decline in the production of the dermal matrix, UV-A (320-400 nm) photoaged skin is characterized by alterations in the dermal matrix. These alterations include the accumulation of the elastic fibers (elastin, fibrillin, desmosine) in deep dermal layers of the skin replacing the collagenated dermal matrix (elastosis), an increase in glycosaminoglycans, collagen cross-linking, epidermal thickening and an increase in the number of dermal cysts [4].

The unifying pathogenic agents for these visible and histological changes are believed to be the UV-generated reactive oxygen species (ROS) that deplete and damage non-enzymatic and enzymatic antioxidant defense systems of the skin as well as causing permanent changes to DNA [30].

The natural ageing of the skin is then probably accentuated by absorption of UV-A radiation by some of the skin chromophores (like for example riboflavin or urocanic acid) which then sensitize the formation of the reactive oxygen species such as singlet oxygen, hydrogen peroxide, and the superoxide anion. These reactive oxygen species then favor chemical reactions like the oxidation of lipids and proteins within the skin [4] and are called oxidants or free radicals.

Nowadays the role of antioxidants in emphasized when dealing with free radicals. Antioxidant is any substance that even when present at relatively low concentrations can significantly delay or inhibit the formation of an oxidant [31]. Antioxidants are for example ascorbate, tocopherol, and carotenoids [32] which are contained in fruits and vegetables.

2.3 Optical Properties of Skin

Spectroscopy of the skin is used in this project to assess changes in the structure and in the properties of the skin, during the course of climate therapy. In particular, measurements of diffuse skin reflectance in the visible and near infrared part of the spectrum are to be carried out to monitor the skin during the treatment. When light illuminates a material, part of it is specularly reflected from the material's surface, while the rest then passes into the material. Specularly reflected light bears information only about the very surface of the material. Within the material, the light interacts with the matter and its molecules,

and can be absorbed or scattered. The shapes of the reflectance and absorption spectra depend on chemical and physical composition of the material, on the size of particles that take part in scattering and on the nature of chromophores causing the absorption [9]. The main principle of diffuse skin reflectance is the analysis of the light as a function of wavelength that has been emitted, reflected or scattered from the material. The particles that interact with the radiation can be defined by the total cross section of the particle, which is used to quantify the probability of interaction between the light and the skin particles:

$$\sigma_t = \sigma_s + \sigma_a \tag{2.1}$$

where σ_s represents the *scattering cross section* and σ_a is the *absorption cross section*.

2.3.1 Reflection

Reflection in the skin is caused by different refractive indices (which vary in skin approximately from 1.33 to 1.55) of the different inhomogeneities in skin [9].

The refractive index n of a medium is defined as the ratio of the speed c of a light wave in a reference medium (vacuum) to the phase speed v_p of the wave in the medium $n = c/v_p$. Refractive index can also be expressed as $n = \sqrt{\varepsilon_r \mu_r}$ where ε_r is the relative permittivity (resistance towards electric field in the media) and μ_r is relative permeability (resistance towards magnetic field of the media) [33].

2.3.2 Absorption

Absorption occurs due to chromophores. Chromophores are molecules' functional groups that cause a conformational change of the molecule when hit by a photon of particular energy. This photon is absorbed by exciting an electron. The same functional groups in different molecules can absorb radiation with different wavelengths, dependent on the energy the electron needs for excitation [34]. Absorption in a homogeneous non-scattering medium can be described with the use of Lambert-Beer's Law;

$$I(x) = I_0 \cdot e^{-\mu_a x} \tag{2.2}$$

where I_0 is the incident intensity, μ_a is the absorption coefficient of the medium and x is the depth within the medium. Absorption is caused by resonant interactions between the molecules energy levels and incident light energy.

2.3.3 Scattering

Scattering is the deflection of incident light due to a change in the refractive index and dependent on the size of the scatterer particle [35].

Each time the light is scattered it moves in a new direction and depending on the amount of scattering particles the photon will travel a given distance between the scattering events. We can define the *mean free path length* l_s in terms of scattering coefficient μ_s by $l_s = \mu_s^{-1}$.

Angular distribution of the scattering angles can be described by *the anisotropy factor*, which is represented by the average cosine of the scattering angle $g = \overline{cos\theta}$. In the skin the scattering is known to be strongly forward directed with $g \approx 0.8$, with experimentally determined wavelength dependence of *the anisotropy factor* given by:

$$g = 0.62 + 29 \cdot 10^{-5} \cdot \lambda \tag{2.3}$$

According to the size of the particle we can distinguish between Rayleigh scattering and Mie scattering, discussed in sections 2.3.3.1 and 2.3.3.2 respectively. The depth where the photons have lost the information about their incident direction is called *the reduced scattering mean free path*

$$l'_s = \frac{l_s}{1-g} = \frac{1}{\mu'_s} \tag{2.4}$$

where μ'_s is the *reduced scattering coefficient*, which takes into account the *anisotropy factor* g. *The transport coefficient* then describes the effective total attenuation

$$\mu_{tr} = \mu'_s + \mu_a \tag{2.5}$$

Scattering is highly influenced by wavelength. Highly energetic short wavelength photons (290 - 400 nm) undergo strong scattering. Longer wavelength photons (600 - 1200 nm) may be transmitted to depths of 0.5 to 2 mm to the tissue. Photons can be scattered due to inhomogeneous distribution of lipids, water and proteins within each cell [10].

2.3.3.1 Rayleigh Scattering

rayleigh scattering occurs when the scattering particle is smaller than the wavelength of the incident radiation. For example, sub-cellular biological structures like mitochondria are Rayleigh scatterers. The scattering cross section is proportional to r^2/λ. This scattering strongly influences the skin reflectance spectra. For example with older age and loss of collagen the scattering in especially the shorter wavelengths (up to 550 nm) drops and elderly people show flatter spectra in this region [36].

2.3.3.2 Mie Scattering Theory

This theory applies when the size of the particle is larger than the wavelength. At this size the electric and magnetic fields of the particles must be considered. This scattering is inversely dependent on the square of the particle radius and depends weakly on the wavelength. One example of this kind of scattering is scattering by water droplets in clouds.

2.3.3.3 Optical Properties of Blood

The optical properties of blood are determined by mostly hemoglobin absorption, in both of its forms oxyhemoglobin and deoxyhemoglobin, and thats why hemoglobin absorption coefficient depends strongly on oxygenation. Blood absorption coefficient is then expressed:

$$\mu_{a,b} = \sigma_{a,b} + \frac{H}{\nu_e} \tag{2.6}$$

where ν_e is the volume percentage of red blood cells erythrocytes, $\sigma_{a,b}$ is the absorption cross section of the blood and H is the hematocrite, the fraction of the blood that is formed by cells. The hematocrite in males is usually 40 - 52% in females 38-48% [13].

The blood *scattering coefficient* is

$$\mu_{s,b} = \sigma_{s,b} + \frac{H(1-H)\cdot(1.4-H)}{\nu_e} \tag{2.7}$$

where $\sigma_{s,b}$ is the *scattering cross section.*

The blood *reduced scattering coefficient* is

$$\mu_{s,b} = \sigma_{s,b} + \frac{H(1-H)\cdot(1.4-H)}{\nu_e} \cdot (1-g_b) \cdot (\frac{685}{\lambda})^{0.37} \tag{2.8}$$

where g_b is the blood anisotropy factor and the last term $(\frac{685}{\lambda})^{0.37}$ is the wavelength dependent scattering approximation determined by the Mie theory.

2.3.3.4 Background Tissue Absorption and Scattering

Absorption caused by factors other than those already mentioned factors can be compared to the absorption observable in ocular tissue and can be approximated with μ_n =25 m^{-1} [37].

Background tissue scattering is caused by the differences in the index of refraction between the collagen fibers and the surrounding tissue and is important for the appearance and color of the skin. The background tissue reduced scattering coefficient is given by [10]:

$$\mu'_{s,n} = C_{Mie} \cdot (1 - 1.7 \cdot 10^{-2}\lambda + 9.8 \cdot 10^{-7}\lambda^2) + C_R\lambda^{-4} \tag{2.9}$$

2.3.3.5 Total Skin Absorption and Scattering Coefficients

The epidermis absorption coefficient is determined as:

$$\mu_{a,e} = \mu_{a,b} \cdot B_e + (\mu_{a,m} + \mu_n) \cdot (1 - B_e) \tag{2.10}$$

where $\mu_{a,m}$ is melanin absorption coefficient and B_e is the blood volume fraction in epidermis.

The epidermis reduced scattering coefficient is given as:

$$\mu'_{s,e} = \mu'_{s,n} \cdot (1 - B_e) + \mu'_{s,b} \cdot B_e \tag{2.11}$$

The dermis absorption coefficient is:

$$\mu_{a,d} = \mu_{a,b} \cdot B_d + \mu_{a,br} \cdot B_{br} + \mu_{a,met} \cdot B_{met} + \mu_{a,beta} \cdot B_{beta} + \mu_n(1 - B_d) \tag{2.12}$$

where B_d is the blood volume fraction in the dermis, B_{br}, B_{met}, B_{beta} are the volume fractions of bilirubin, methemoglobin and betacaroten respectively. $\mu_{a,br}$, $\mu_{a,met}$, $\mu_{a,beta}$ are the absorption coefficients for bilirubin, methemoglobin and betacaroten respectively.

Finally the dermis reduced scattering coefficient:

$$\mu'_{s,d} = \mu'_{s,n} \cdot (1 - B_d) + \mu'_{s,b} \cdot B_d \tag{2.13}$$

2.4 Psoriasis

Psoriasis is a common autoimmune skin disease with inflammatory symptoms. Its prevalence is estimated at 1.3 percent of the global African American population and 2.5 percent of Caucasians, which accounts to 125 million people worldwide [38]. It affects the patients' quality of life, social interactions and has worldwide economical impact.

(a) Patient A (b) Patient B

FIGURE 2.6: Patients with psoriasis (photos courtesy of Anne-Lene Krogstad, Oslo University Hospital).

Psoriasis can have different forms: psoriasis vulgaris (the most common plaque type), guttate psoriasis (small, individual spots), inverse psoriasis (smooth red lesions in the

folds of the skin), pustular psoriasis (white non-infectious pus - blisters filled with dead white blood cells), palmoplantar psoriasis (found on palms and soles) and erythrodermic (affecting most of the body) [39]. Another form this disease can take is psoriatic arthritis, a form of psoriasis that affects joints. It can appear separately or in conjunction with skin psoriasis (preceding or following after). Its symptoms are similar to other arthritic diseases.

2.4.1 Mechanisms Behind Psoriasis

Several different factors take part in developing psoriasis lesions [40]. The immune system is strongly involved with genetic predispositions and external or internal triggers.

The lesions are formed by quickly proliferating keratinocytes which are stimulated by inflammatory signals from T lymphocytes. In normal skin development the skin cell is formed, matures, loses its nuclei and falls off in 28 day cycles. The stimulated keratinocytes have 3 to 4 day cycles, which causes thickening of the skin. The keratinocytes in the plaques do not lose their nuclei. Simultaneously these cells also fail to produce the lipids necessary to adhere the skin cells together. This results in the formation of the typical psoriatic scales. Due to inflammatory cytokines produced within the plague, the mentioned psoriatic keratinocytes are resisting the apoptosis. The psoriatic erythema is caused by dilated dermal blood vessels near the skin surface that nurture the keratinocytes.

It is known that psoriasis is more likely to occur in genetically susceptible individuals while triggered by endogenous or exogenous stimuli [40]. In the psoriatic lesions epidermis is infiltrated by CD8+ T cells, while CD4+ T cells are concentrated in the upper dermis, these cells are responding to specific antigens and seem to be involved in the pathogenic process of psoriasis. One well defined external cause that might initiate psoriasis is throat infection with $\beta-$haemolytic streptococci. T cells then respond to certain amino acids that the keratins (fibrous structural proteins contained in keratinocytes) share with the streptococcal proteins.

It has been proven that part of the CD4+ T cells in the lesions are the regulatory T cells which restrict the memory of CD8+ T cells (their memory of amino acid antigen) and their depletion causes lesion expansion [40]. It is believed that CD4+ T cells evoke the disease and CD8+ T cells are the executors, the changes in the severity of the lesions may be the result of changes in the balance between the regulatory T cells and CD8+ T cells [40].

2.4.2 Evaluation of Psoriasis

For our needs the patient's psoriasis will be defined by its severity. The severity of the lesions and their properties are defined by the dermatologist and expressed by the PASI index. Psoriasis Area Severity Index (PASI) is computed as follows [41]. The psoriatic lesions are evaluated based on three criteria: redness (erythema E), thickness (Induration I), and scaliness (Desquamation D), having scale from 0 (least) - 4 (worst). The body is divided into four parts: the head (h), the arms (a), the trunk (t), and the legs (l) each of

these is multiplied by a weight factor to express their skin area proportion to the whole body. The area of the body parts involved in the psoriatic lesions is expressed by A factors with values 0 (none) to 6 (maximum).

$$PASI = 0.1 \cdot (E_h + I_h + D_h) \cdot A_h + 0.2 \cdot (E_a + I_a + D_a) \cdot A_a + \\ +0.3 \cdot (E_t + I_t + D_t) \cdot A_t + 0.4 \cdot (E_l + I_l + D_l) \cdot A_l \tag{2.14}$$

The PASI index can go from 0 (no signs) to a maximum value of 72. For our problem we will use the division into mild psoriasis PASI 1-7 , moderate PASI 7-12 and severe psoriasis PASI 12 and above [41].

2.5 Possible Psoriasis Treatments

Nowadays the treatment of psoriasis focuses on dealing with the immunity manifestations in the plaques [39]. It aims to regulate the inflammatory processes in the lesion and in this way reduce the keratinocytes' proliferation and cure the site. For example steroids have anti-inflammatory, antiproliferative, immunosuppressive and vasoconstrictive effects. They are able to alter genes responsible for the production of inflammatory cytokines. This automatically reduces all the other lesion symptoms, albeit at a cost of significant side effects like skin atrophy, and their extensive or longer use may even lead to systemic side effects. An alternative to the use of topical corticosteroids may be topical vitamin D analogue.

Vitamin D is responsible for the regulation of calcium uptake in the intestine and its management in the bones, but can also stop cellular proliferation and stimulate cellular differentiation in keratinocytes. It binds to intracellular receptors that later interacts with DNA leading to transcriptional changes. Vitamin D alone is not used since there is a risk of developing hypercalcemia, instead for example the analogues of vitamin D_3 are applied in the form of topical treatment. When the doses are kept low, there are no reported systemic side effects. However, some users may experience irritation [39].

2.5.1 Erythema

It is important to distinguish between two types of erythema relevant to this paper. The first is erythema of psoriatic plagues which is caused by dilated dermal blood vessels near the skin surface that nurture the keratinocytes as mentioned above in section 2.4.1. The second one is symptomatic of excessive sun exposure. This may result in chronic responses like skin aging and skin cancer referenced in section 2.5.2, and to an acute response - sunburn (in this paper referred as sun-caused erythema), which consists of three phases. First phase is vascular dilatation and edema, second is inflammatory phase and the last is regressive anti - inflammatory phase. Various types of cells and biochemical processes take part in the last two phases [42].

2.5.2 UV Radiation

It is known that the aforementioned inflammatory and immunological processes in the skin which are causing the psoriasis can be influenced by applied UV irradiation [40]. UV radiation is one part of the solar radiation spectra from 200 - 400 nm, divided into UVC (200 - 280 nm), UVB (280-315 nm) and UVA (315-400 nm) according its biological effects.

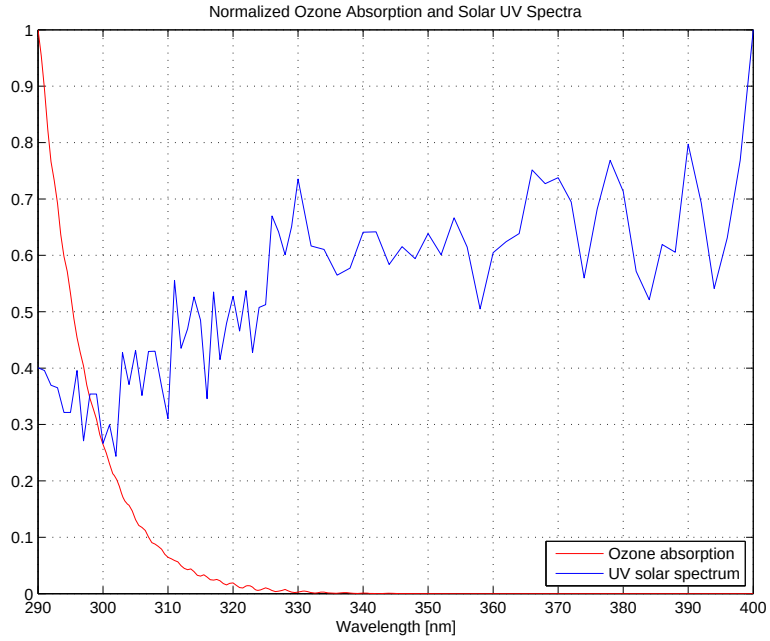

FIGURE 2.7: Normalized UV solar spectrum and ozone absorption spectrum, (data courtesy of Dr. Vitali Fioletov, Science and Technology Branch Environment Canada).

All UVC and also some of the UVB is effectively blocked by the ozone layer. The rest of UVB in excessive amounts is responsible for erythema and together with UVA for DNA mutations and skin cancer. UVA can cause erythema as well but much higher doses are required. UVB is mainly absorbed in the epidermis. The longer wavelengths in the UVA range penetrate deeper into the skin and reach the dermis where they are responsible for premature skin aging effects [43] [44]. The UV radiation spectrum together with ozone absorption spectrum is illustrated on figure 2.7.

Only a part of the UV spectra is considered having effect on biological material and thus on human skin. The biologically active radiation erythema causing spectrum is given by the overlap of the spectral irradiance and the erythemal action spectrum [45] [46].

Since most of the UVB radiation does not penetrate into the dermis, broadband UVB preferentially reduces the epidermal T cells and only part of its photons penetrate deep enough to deplete also some of the dermal T cells [47]. T cells (preferably CD8+ T cells) are much more sensitive to UVB radiation than keratinocytes.

Psoralen plus UVA (PUVA) is another psoriasis treatment based on illumination of the skin by UVA radiation after administrating the skin with a photosenzitizer. UVA radiation needs much higher doses to clear the psoriasis and its practical use is limited to

combinations with photosensitizing agents like psoralen, found in plants [48]. This method is more potent for deeper treatment and is able to reduce both dermal and epidermal T cells involved in the psoriasis mechanism. PUVA is more effective, with long psoriasis remission times, although the therapy has serious systemic side effects like patient swelling, nausea and photosensitivity. The treatment also causes an increased risk of non-melanoma and melanoma skin cancer [49].

To avoid the side effects and risks connected to PUVA, UVB radiation is preferred in the psoriasis light treatment nowadays. Traditionally UVB light was administered in the form of the whole UVB spectra (280-315 nm) called broadband UVB. Later studies proved that psoriasis can be treated successfully with wavelengths 304 - 311 nm. This narrow-band UVB leads to clearing of psoriasis allowing the doses to be sub-erythemogenic, having higher therapeutic effect at lower doses. This is in contrast to broadband UVB that contains wavelengths which have no psoriasis therapeutic effect but cause erythema, limiting the maximum dose that can be administered to the patient [50]. The effect of UVB radiation treatment can be enhanced by simultaneous application of topical treatments such as vitamin D3 analogues.

2.6 UV Dose

To make the stay in the climate therapy center most efficient it is necessary to decide what dose has the best treatment results with the lowest risk possible. The amount of the incident UV radiation is usually expressed as the incident energy on a surface in J/m^2 within some time. Other units can found in the literature which are relevant for illumination of tissue and its erythemal response. The following table summarizes these units and gives their equivalent values in J/m^2.

Unit		**Incident energy [J/m^2]**
Standard Erythema Dose	SED	100
Minimal Erythema Dose	MED	Individually varies
Erythemal Unit	EU	280

TABLE 2.2: Incident UV radiation units [51].

Minimal erythema dose is the amount of energy from the radiation that causes the first perceptible erythema; its value varies with different skin types [52]. The first observation of erythema on a skin that is not usually exposed to sun are after 1.5 SED in Fitzpatrick's skin type I , 2 SED in type II and 3 SED in III [53, 26].

2.7 Model Theory of Light Interaction with Skin

To be able to predict the effects of skin exposure to light, we need to describe and quantify this interaction with a mathematical model. Skin tissue is a very complex structure and various simplifications must be considered in order to fit it to a model. When studying skin morphology in more detail we can recognize various layers. To achieve better accuracy of the model, this can also be further divided in parts each describing a different layer, and the relation to adjacent layers.

2.8 Radiative Transfer Theory

Radiative transfer theory describes the flow of the light power through a turbid medium. This theory is valid if we treat photons as tiny particles that interact with absorbing and scattering particles, which applies under following assumptions:

- We assume no coherence between scattered electric fields and negligible diffraction and coherence.
- Photons are assumed being absorbed or elastically scattered by the medium particles. We suppose that wavelength effects like Raman scattering and fluorescence emission are negligible.
- Light is assumed to be random polarized.

The following quantities will be used in the description of light transfer [54]:

2.8.1 Radiant Power P

is the power emitted, transferred or received as radiation expressed in Watts.

2.8.2 Radiant Intensity I

is the light power emitted by source in a given direction $I = \frac{dP}{d\Omega}$, where $d\Omega$ is the element of solid angle. The units are W/Sr.

2.8.3 Radiance L

is the amount of light that passes through a point in a given direction in $WSr^{-1}m^{-2}$, illustrated on figure 2.8. It describes the angular and spatial distribution of light in tissue.

$$L = \frac{dI}{dA \cdot cos\theta} \tag{2.15}$$

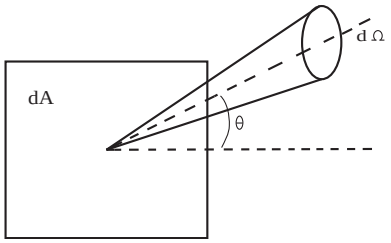

FIGURE 2.8: Radiance formula graphical representation. Radiant intensity dI of an element dA of a surface divided by an orthogonal projection of this element on a plane perpendicular to a given direction, $d\Omega$ is the element of solid angle, θ is the angle between the different directions of incidence and the normal to the surface.

2.8.4 Irradiance E

is the radiant intensity incident on an element of the surface divided by the area of the element, and describes the total power incident from a hemisphere on that area in Wm^{-2}.

$$E = \int_{2\pi} L(s) \cos\theta d\Omega \tag{2.16}$$

where θ is the angle between the different directions of incidence and the normal to the surface.

2.8.5 Fluence Rate ϕ

is the total light power that passes through a point [54], given from section 2.8.3:

$$\phi(r) = \int_{4\pi} L(\omega, r) d\Omega \tag{2.17}$$

When light hits an absorbing material, the total light absorption is proportional to the absorber particle concentration ρ and the cross section of a single absorber σ_a. The total absorption cross section of a material with thickness dx and particle concentration ρ is given by $\rho\sigma_a dx$.

The power ϕ is attenuated as light passes through the material, at a rate given by:

$$\phi = \phi_0 \rho \sigma_a dx \tag{2.18}$$

where $\rho\sigma_a$ is the absorption coefficient μ_a as in section 2.3.2. By integrating the above mentioned equation we can obtain Beer's law for absorption:

$$\phi(x) = \phi_0 e^{-\mu_a x} \tag{2.19}$$

which states that the incident power flux is reduced by a factor of e^{-1} on a pathlength of μ_a^{-1}. If the scattering contribution is small ($\rho\sigma_s x \ll 1$) [54] scattering can also be described by Beer's law

$$\phi(x) = \phi_0 e^{-\mu_s x} \tag{2.20}$$

Hence the combined effect is:

$$\phi(x) = \phi_0 e^{-\mu_t x} \tag{2.21}$$

where $\mu_t = \mu_a + \mu_s$ is the total attenuation coefficient. From these conclusions we can derive *the scattering* and *absorption mean free paths*. The probability that a photon will reach depth x is:

$$\frac{\phi(x)}{\phi_0} = e^{-\mu_a x} \tag{2.22}$$

the probability that this photon is absorbed on a distance dx from x is:

$$\frac{-d\phi(x)}{\phi(x)} = \mu_a dx \tag{2.23}$$

Then the probability $p_a dx$ that the photon will be absorbed on interval [x, x + dx] is the product:

$$p_a(x)dx = \mu_a e^{-\mu_a x} dx \tag{2.24}$$

which gives the probability distribution function for absorption, hence the average distance a photon can travel is:

$$l_a = \int_0^\infty x p_a(x) dx = \mu_a \int_0^\infty x e^{-\mu a x} dx \tag{2.25}$$

and $\mu_a = 1/l_a$.

2.8.6 The Boltzman Transport Equation

When light is exposed to multiple scattering, a more complicated description of light transport is necessary. For this purpose the *Boltzman Transport Equation* can be used – partial differential equation of the radiance L and it describes the propagation of electromagnetic waves in scattering media [55, 56]. The probability of interaction with tissue is quantified by two parameters; the linear scattering and absorption coefficients in $[m^{-1}]$. It expresses the photon migration by the balance of light power.

$$\frac{1}{c}\frac{\partial L(r,\vec{s},t)}{\partial t} + \nabla L(r,\vec{s},t)\cdot\vec{s} = \tag{2.26}$$
$$= -(\mu_s+\mu_a)L(r,\vec{s},t) + \mu_s \iint_{4\pi} L(r,\vec{s}\,',t) f(\vec{s},\vec{s}\,')d\omega + Q(r,\vec{s},t)$$

where $\vec{s}$ is the unit vector pointing in the direction of interest and $f(\vec{s},\vec{s}\,')$ is the normalized differential scattering cross section.

- $\iint_{4\pi} f(\vec{s},\vec{s}\,')d\omega = 1$ and describes the probability of a photon with direction $\vec{s}$ being scattered into direction $\vec{s}\,'$ in a scattering event.
- The terms $\frac{1}{c}\frac{\partial L(r,\vec{s},t)}{\partial t} + \nabla L(r,\vec{s},t)\cdot\vec{s}$ give the sum of temporal change and spatial change of light power passing through a small volume at r in direction $\vec{s}$.
- $-(\mu_s+\mu_a)L(r,\vec{s},t)$ represents the loss of light power and is the fraction of light power that enters the volume and becomes either absorbed in or scattered out of direction $\vec{s}$.
- $\mu_s \iint_{4\pi} L(r,\vec{s}\,',t) f(\vec{s},\vec{s}\,')d\omega$ is the amount of light power that enters the volume in direction $\vec{s}\,'$ and is deflected into direction $\vec{s}$ by scattering and represents gain of light power.
- $Q(r,\vec{s},t)$ is the radiant intensity of a source within the volume emitting light into direction $\vec{s}$ and represents the gain.

The equation treats photons as balls undergoing elastic collisions and traveling through the medium at speed $c = \frac{3\cdot 10^8}{n} m/s$ where n represents the refractive index, its value for skin tissue is 1.4 [9].

The transport equation takes the general form of a continuity equation, when integrated over all solid angles [57]:

$$\frac{1}{c}\frac{\partial\phi(r,t)}{\partial t} + \nabla j(r,t) = -\mu_a\phi(r,t) + S(r,t) \tag{2.27}$$

$$\begin{aligned} S(r,t) &= \iint_{4\pi} Q(r,\vec{s}\,',t)d\omega \\ \phi(r,t) &= \iint_{4\pi} L(r,\vec{s}\,',t)d\omega \\ j(r,t) &= \iint_{4\pi} L(r,\vec{s}\,',t)\vec{s}d\omega \end{aligned} \tag{2.28}$$

When scattering is much stronger than absorption ($\mu_s \gg \mu_a$) the radiance can be expressed as an isotropic fluence rate ϕ plus small directional flux j and the transport equation reduces to the *diffusion approximation* [10, 9]:

$$L(r,\vec{s},t) = \frac{1}{4\pi}\phi(r,t) + \frac{3}{4\pi}j(r,t)\vec{s} \tag{2.29}$$

Substituting the *diffusion approximation* equation 2.29 in *the transfer equation* equation 2.26, multiplying by $\vec{s}$ and integrating over all solid angles gives:

$$\frac{1}{c}\frac{\partial j(r,t)}{\partial t} = -\frac{1}{3}\nabla\phi(r,t) - \frac{1}{3D}j(r,t) \tag{2.30}$$

where D is the photon diffusion coefficient $D = \frac{1}{3[(1-g)\mu_s-\mu_a]} = \frac{l_{tr}}{3}$ and l_{tr} is *the transport mean free path*. For an isotropic source Q in steady state *Fick's law* applies:

$$j(r) = -D\nabla\phi(r) \tag{2.31}$$

Which inserted in the steady state version of equation 2.27:

$$\nabla j(r) = -\mu_a\phi(r) + S(r) \tag{2.32}$$

gives us *the steady state diffusion equation*:

$$D\nabla^2\phi(r) - \mu_a\phi(r) = -S(r) \tag{2.33}$$

The optical penetration depth is defined as:

$$\delta = \sqrt{\frac{1}{3\mu_a\mu_{tr}}} \tag{2.34}$$

and it is the depth inside the material at which the intensity of the light radiation falls to $1/e$ of the original value at the surface [33].

2.8.6.1 Boundary Conditions for the Transport Equation

The continuity of irradiance in the forward and backward directions must be preserved between two scattering media where there is no accumulation [10]:

$$\begin{aligned} \frac{\phi_1}{4} + \frac{j_1}{2} &= \frac{\phi_2}{4} + \frac{j_2}{2} \\ \frac{\phi_1}{4} - \frac{j_1}{2} &= \frac{\phi_2}{4} - \frac{j_2}{2} \end{aligned} \tag{2.35}$$

To get the boundary condition between air and tissue we equate the reflected part of the radiation at the tissue/air boundary to the radiation propagating back into the skin.

$$R_{eff}(\frac{\phi}{4} + \frac{j}{2}) = \frac{\phi}{4} - \frac{j}{2} \tag{2.36}$$

where R_{eff} is the effective reflection coefficient; for the refractive index n=1.4 $R_{eff} = 0.493$. For this boundary conditions to be valid the flux j has to be less than the fluence rate ϕ.

2.8.6.2 Source Functions and Solutions

The model used in this project is a three layer model further described in 4, for simplicity mathematical description of two layer model will be given in this section.

For the two layer skin model the skin is divided in between an epidermal layer with finite thickness d_e and a semi - infinite dermal layer. A small amount of the incident light is specularly reflected at the surface, the remainder is transmitted into the tissue. The transmitted light is multiply scattered in the tissue and will eventually obtain an isotropic distribution. The source functions for epidermis and dermis are respectively:

$$\begin{aligned} g_e &= P_t\mu'_{s,e}e^{-\mu_{tr,e}x} & 0 < x \leq d_e \\ g_d &= P_t\mu'_{s,d}e^{-\mu_{tr,e}d_e}e^{-\mu_{tr,d}(x-d_e)} & d_e < x \leq \infty \end{aligned} \tag{2.37}$$

where P_t is the transmitted fraction of the incident light, and $\mu'_{s,e} = \mu_{s,e}(1-g)$, $\mu'_{s,d} = \mu_{s,d}(1-g)$ are the reduced scattering coefficients in epidermis and dermis respectively.

The fluence rates are then:

$$\phi_e = \frac{P_t \delta_e^2 \mu'_{s,e}}{D(1-\mu_{tr,e}^2 \delta_e^2)} + e^{-\mu tr,ex} + A_1 e^{-\frac{x}{\delta_e}} + A_2 e^{-\frac{x}{\delta_e}} \tag{2.38}$$

$$\phi_d = \frac{P_t \delta_d^2 \mu'_{s,d}}{D(1-\mu_{tr,d}^2 \delta_d^2)} + e^{-\mu tr,ed_e} + e^{-\mu_{tr,d}(x-d_e)} + A_3 e^{-\frac{x}{\delta_d}} \tag{2.39}$$

constants A_1, A_2 and A_3 can be found by applying the boundary conditions. The effective reflection coefficient R_{eff} can be found by integrating the expression for Fresnel reflection coefficient with respect to all angles of incidence from the inside of the medium. For non polarized light:

$$R_\phi = 2 \int_0^{\pi/2} \sin(\theta)\cos(\theta) R_F(\theta) d\theta \tag{2.40}$$

$$R_j = 3 \int_0^{\pi/2} \sin(\theta)\cos^2(\theta) R_F(\theta) d\theta \tag{2.41}$$

$$R_F(\theta) = \begin{cases} \frac{1}{2}\left(\frac{n\cos\theta' - n_{out}\cos\theta}{n\cos\theta' + n_{out}\cos\theta}\right)^2 + \frac{1}{2}\left(\frac{n\cos\theta - n_{out}\cos\theta'}{n\cos\theta + n_{out}\cos\theta'}\right)^2 & 0 \le \theta \le \theta_c \\ 1 & \theta_c \le \theta \le \frac{\pi}{2} \end{cases} \tag{2.42}$$

$$R_F(\theta = 0) = \left(\frac{n - n_{out}}{n + n_{out}}\right)^2 \tag{2.43}$$

Where θ is the angle of incidence from inside the tissue and is given by $cos\theta = s \cdot n$, $\vec{s}$ being the direction of incidence to the surface. θ' is the scattering angle in the medium outside and it satisfies the Snell's law, $n \sin\theta' = n_{out} \sin\theta$. θ_c is the critical angle for total internal reflection and is given by $n \cdot \sin\theta_c = n_{out}$. For normal incidence we can simplify:

$$R_{eff} = \frac{R_\theta + R_j}{2 - R_\theta + R_j} \tag{2.44}$$

Part II

Methods and Instrumentation

3

Skin Spectroscopy

Skin spectroscopy consists of illuminating the subject skin with light and recording the light returning back from the skin to the detector. This can be done with the use of a probe in the form of an integrating sphere, or with a fiber optic probe. The collected light is then forwarded to a spectrometer. The working principle of the spectrometer is further discussed in section 7.2. The spectrometer sends the collected data to a computer through an USB port. In the computer the spectroscopic data acquisition is operated by a software application, in this case either *OOIbase* or *Spectra Suite* which are the standard operating softwares for Ocean Optics instruments, which is the case of the spectrometer used.

Prior to the measurements the light source should be switched on for some time to stabilize on its working temperature. Before each measurement the setup is calibrated with the use of the white standard (described in section 7.4); this is done both with the integrating sphere light source switched on and switched off. Integration time can be selected for the spectra acquisition, in the case of the psoriasis spectra measurements the integration time was set to 18 msec.

Since the skin measurements are very sensitive to blood circulation changes and its oxygenation, it is recommended to keep the patient in a relaxed position before the measurements to achieve eproducible measuring conditions. The skin properties are also affected by ambient temperature and also by body temperature, hence the room temperature should be kept as constant as possible. To obtain the skin spectra the integrating sphere is placed to the skin surface on the desired spot and the spectra is saved through the operating software. The pressure applied to the skin during the measurement should be always kept as low as possible to prevent discoloring or on the contrary erythema in the measured spot. The effects of different pressure on the skin spectra are considerable, as discussed in [9]. For successive measurements the same placement of the sphere is desirable. The spectra is saved in .txt format to ease further handling in the Matlab programming environment. The data file contains a header with all the important settings from when the experiment was taken.

4

Diffuse Skin Model

Based on the radiative transfer theory discussed in section 2.8, Svaasand et al. [58] developed the diffuse skin model. This model has been further developed by [9] and [54].

The three layer version of this model was used for the purpose of this project. The model can be conveniently divided into layers coinciding with structural layers in the skin, at the same time reducing its mathematical complexity relative to a non-layered approach as Monte-Carlo. First layer is simulating the epidermal skin layer and is 80 μm thick. Layers two and three represent the dermal skin layer of thickness 1 mm, where the second model layer is 0.2 mm thick and the third model layer is semi - infinite. The model respects the skin's scattering and absorption properties as described in section 2.3, and takes into account the main chromophore skin constituents mentioned in 2.1.3.

4.1 Model Parameters to Vary

Several parameters can be set up for this model, three of these were selected and are used in the inverse model to define the different measured skin spectra. These include the melanin absorption coefficient at 694 nm (in [m^{-1}]), the blood volume fraction [%] in the second model layer and the oxygenation [%] in the second layer. The influence they have on the spectrum is demonstrated in the following figures, where one parameter at a time is varied with the others constant. The average values used are 500 m^{-1} for the melanin absorption coefficient, 0.5% blood volume in the second layer 80 % for the oxygenation in the second layer.

A higher melanin absorption coefficient decreases the slope of the spectrum and reduces the overall reflectance from the simulated skin due to higher absorption caused by the melanin as demonstrated on figure 4.1. On this figure several melanin spectra are simulated with the use of the diffusion model. Spectra with higher melanin absorption are generally flatter, with the effect visible over the whole range of observed wavelengths from 400 nm to 850 nm.

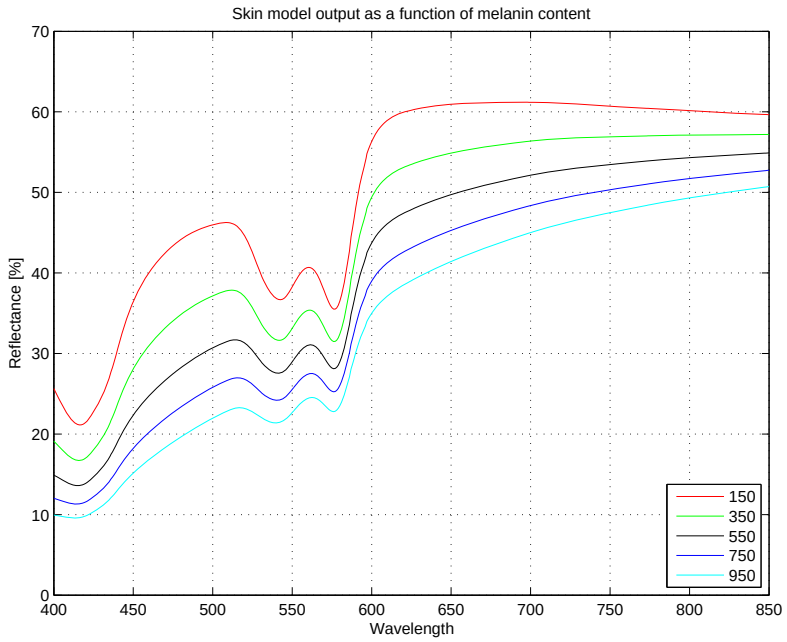

FIGURE 4.1: The effect of changing the melanin absorption coefficient [m^{-1}].

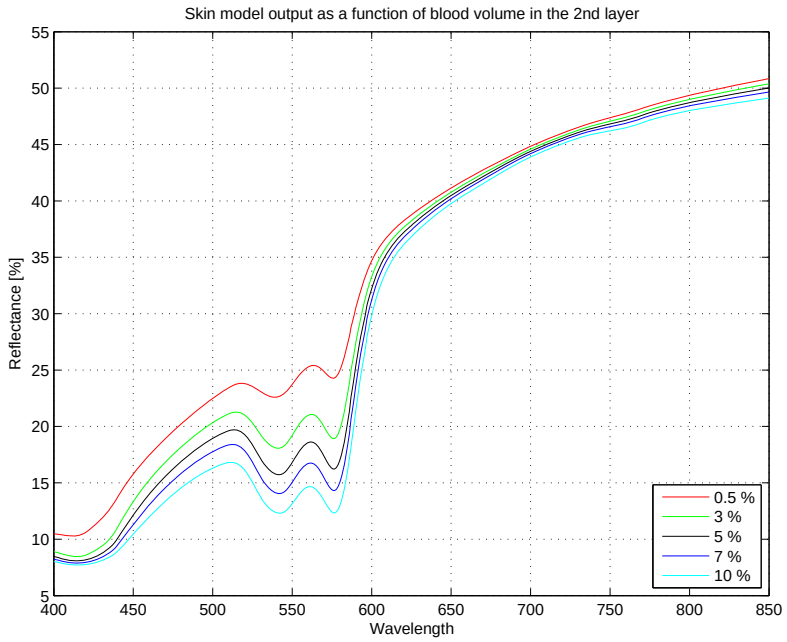

FIGURE 4.2: The effect of changing the blood volume in the second layer of the model.

A higher percentage of blood in the second model layer has the effect of reduced reflectance in the spectra (presented on figure 4.2) due to increased absorption in several blood chromophores as discussed in section 2.1.3. It mainly affects the spectra in the lower half of observed wavelengths up to approximately 580 nm, with the effect on the second half of the spectra seems to be negligible.

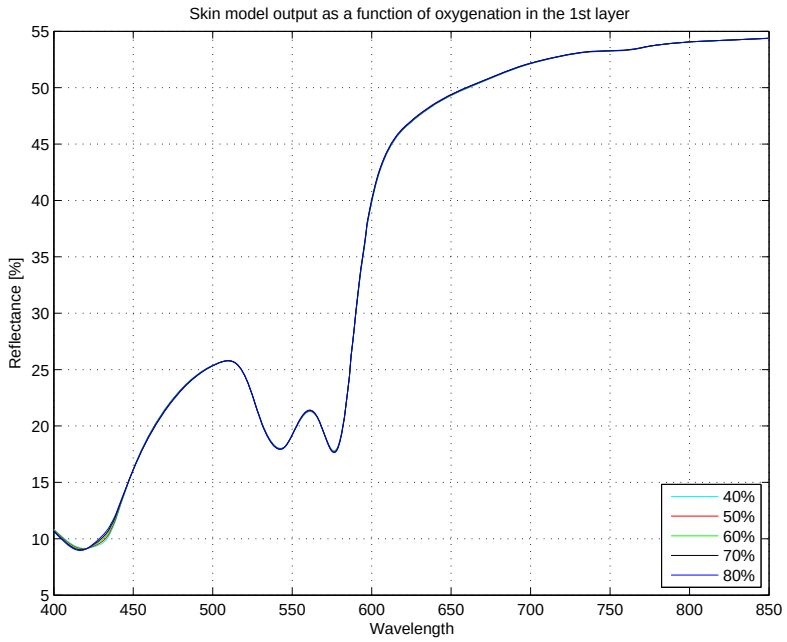

FIGURE 4.3: The very small effect of changing the oxygenation in the first layer of the model.

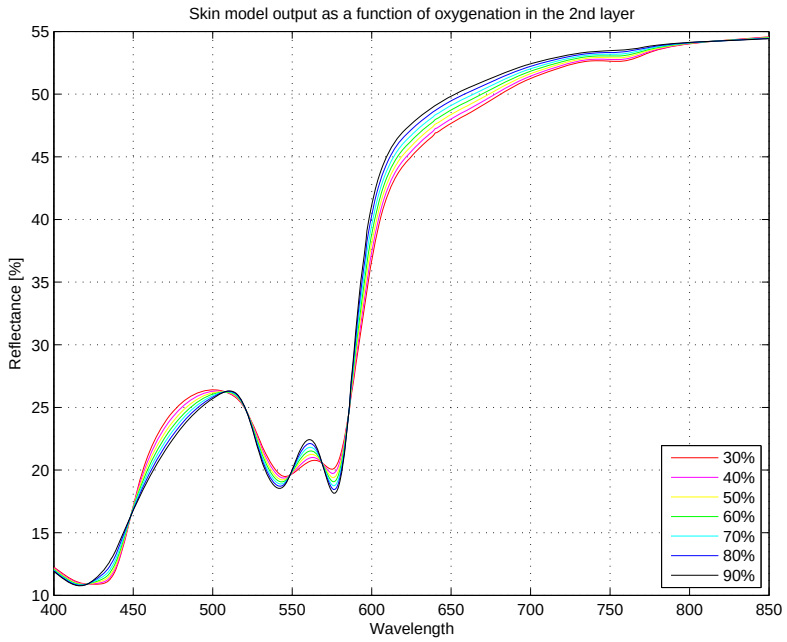

FIGURE 4.4: The effect of changing the oxygenation in the second layer of the model.

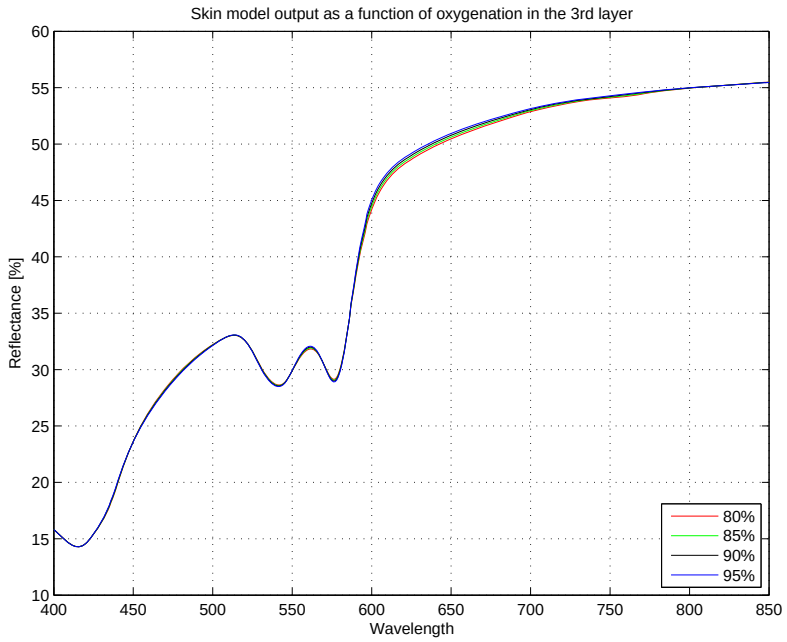

FIGURE 4.5: The effect of changing the oxygenation in the third layer of the model.

The most pronounced effect of oxygenation is in the second model layer as demonstrated on figures 4.3, 4.4 and 4.5, for each case the blood volume, which greatly affects the results of varying oxygenation, was set to 0.6% in every layer.

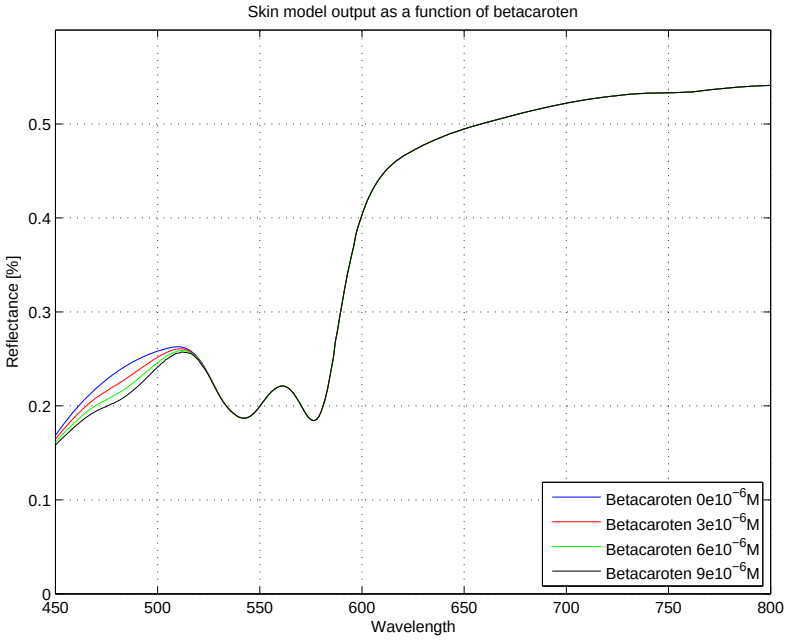

FIGURE 4.6: The effect of changing the betacaroten content.

Betacaroten content in the skin has a big influence on the simulated spectra; even in small amounts it acts as a big absorber and reduces the reflectance of the simulated

spectra. Its main effect can be observed between 430 and 530 nm. Betacaroten rich diet will influence the measurements.

4.2 Parameters Affecting the Model Results

Figure 4.7 illustrates the changes the reflectance spectra exhibits with variation of the scattering coefficients. Standard values (for adult persons) of the Mie and Rayleigh scattering coefficients are 105 cm^{-1} and $1.05 \cdot 10^{12}$ nm^4cm^{-1} respectively [9]. To visually illustrate the trends in the effects of these parameters they were changed to extreme values of 150 cm^{-1} and $5 \cdot 10^{11}$ nm^4cm^{-1} respectively.

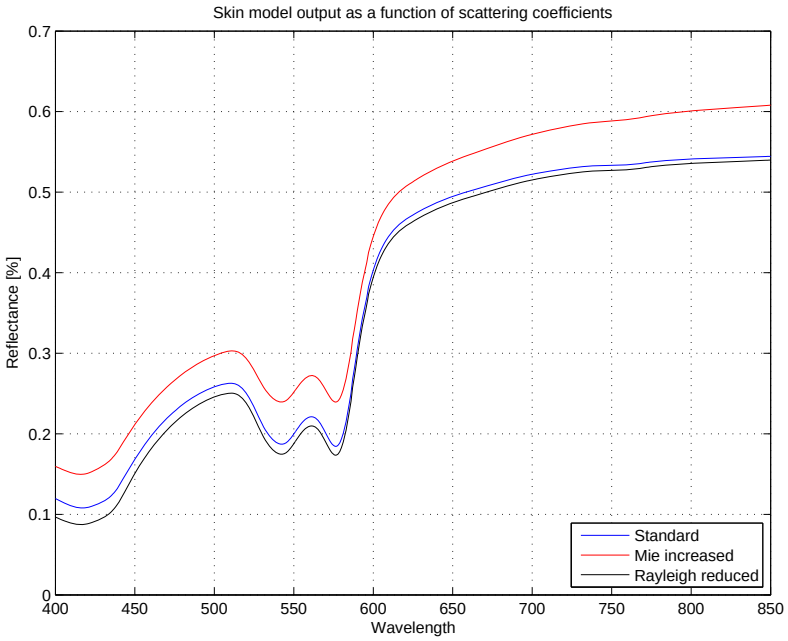

FIGURE 4.7: The effect of changing the scattering coefficients.

A reduced scattering coefficient causes a downwards shift in the reflectance spectrum. Similarly increased scattering increases reflectance for both types of scattering.

4.3 Source Functions

Two source functions are available in the model; Isotropic and δ-Eddington. The isotropic source function assumes that the intensity of the incident light drops exponentially with growing depth in the skin as described by Beer's law (equation 2.2) [54]. The δ-Eddington source function is based on the assumption that tissue scattering is very forward directed and most of the photons are not deflected at all from their trajectory – hence in practice the light is less attenuated by scattering than Beer's law predicts [54].

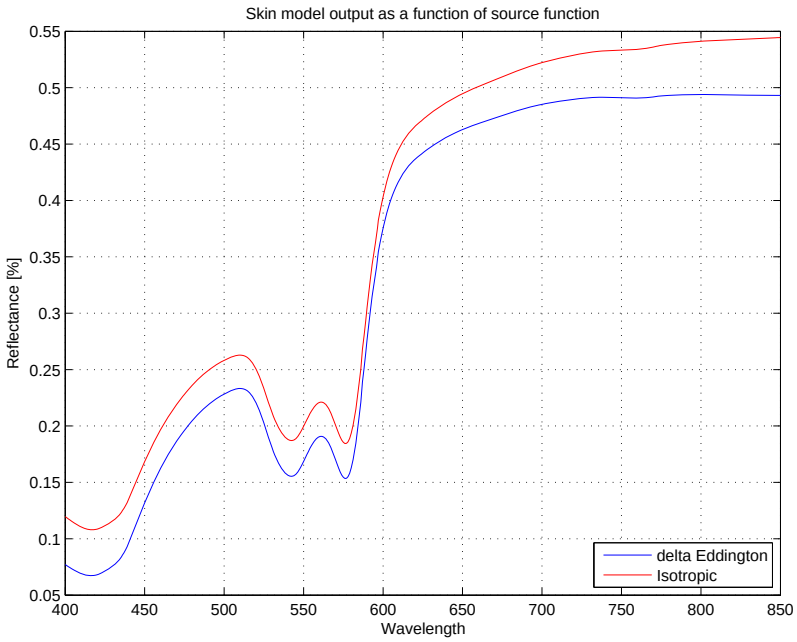

FIGURE 4.8: The modeled spectra for the two different source functions, isotropic and δ-Eddington source function.

For the needs of this project the isotropic source function was used. The results given by these two source functions can be compared on figure 4.8, where only the used function was changed with other parameters held constant. The constant values of the relevant parameters were 80% for oxygenations in all three model layers, melanin absorption coefficient was on an average value of 500 m^{-1} and blood volume in the second model layer was 0.6 %.

5

Characterization of the Spectra

Spectra measured on the patients' skin along with the spectra generated by the diffuse skin model are to be defined by indices describing the skin properties; these will be the melanin index, the hemoglobin index, blood oxygenation and blood volume. Absorption in biological tissues is dominated by water, melanin and hemoglobin.

Even though water is the most abundant molecule in human body it mainly absorbs in the UV and infrared regions of the light and therefore can be neglected for measurements in the visible light region hence it is not considered in the model. The water absorption spectrum for the light wavelength region of interest is illustrated on figure 5.1 [59].

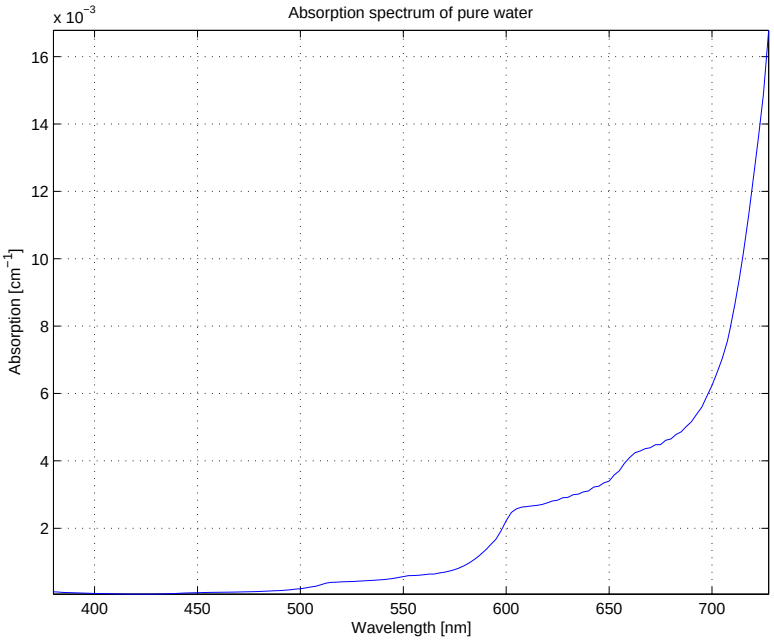

FIGURE 5.1: Water absorption spectrum on 380-700 nm.

5.1 Hemoglobin Index

The extinction coefficient is defined as the probability of photon interaction with the medium per unit path length. Extinction itself includes absorption and scattering, but for hemoglobin absorption dominates.

The molar extinction spectra of oxy and deoxyhemoglobin are different but share a few intersections called *isosbestic points*. An *isosbestic point* is a specific wavelength at which two substances have the same molar extinction coefficient.

At these points the absorption coefficient depends only on the total hemoglobin concentration and not on the oxygen saturation [5]. Figure 9.21 shows the extinction coefficients of oxy and deoxyhemoglobin.

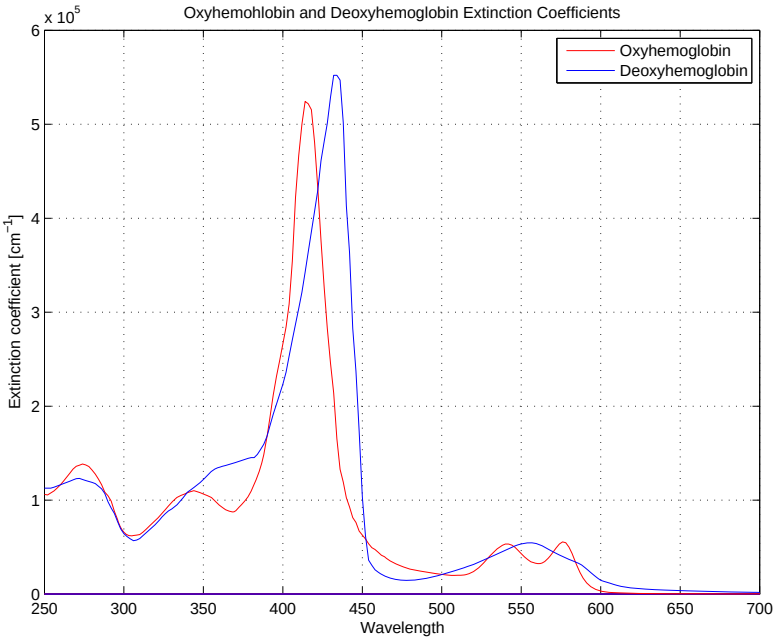

FIGURE 5.2: The oxyhemoglobin and deoxyhemoglobin extinction coefficient curves with isosbestic points [5].

The isosbestic points derived from these curves are at 500, 527, 544, 573 and 584 nm. These can be used in the calculation of the hemoglobin index [60] to describe the relative changes of hemoglobin concentration in the patients skin in the following way:

$$H = \left(\frac{\mu_a(544) - \mu_a(527)}{16.5} - \frac{\mu_a(573) - \mu_a(544)}{29} \right) \cdot 100\% \tag{5.1}$$

where $\mu_a(\lambda)$ are the apparent absorption values at wavelength λ.

5.2 Melanin Index

The slope of the melanin absorbtion spectrum is proportional to the melanin concentration [18]; the slope can be calculated as the difference between the means of the apparent absorption spectra values at 645, 650, 655 and 695, 700, 705 nm, multiplied by a value of 100 to obtain the result in percents. This index describes the pigmentation of the skin.

$$Melanin = \left(\overline{\mu_a(645, 650, 655)} - \overline{\mu_a(695, 700, 705)} \right) \cdot 100\% \tag{5.2}$$

5.3 Blood Oxygenation

The percentage of blood oxygenation is calculated as [61]:

$$Oxygenation = \frac{\mu_{Hb}(\lambda_1) - \mu_{Hb}(\lambda_2) \cdot \frac{\mu_a(\lambda_1)}{\mu_a(\lambda_2)}}{\mu_{Hb}(\lambda_1) - \mu_{HbO_2}(\lambda_1)} \cdot 100\% \tag{5.3}$$

where $\mu_a(\lambda)$ is the measured absorption coefficient at wavelength λ, μ_{Hb} and μ_{HbO_2} are the specific absorption coefficients of deoxygenated and oxygenated hemoglobin respectively. The wavelengths that were used are $\lambda_1 = 542$ and $\lambda_2 = 548$ nm as suggested in [62]. The specific absorption coefficients used were calculated from molar extinction coefficients [cm^{-1}/(moles/liter)] for hemoglobin in water [5]. To convert this data to absorption coefficient in cm^{-1}, the molar extinction coefficient was divided by the molar concentration 64500 gHb/mole and multiplied by a logarithm conversion factor 2.303,

$$\mu_a(\lambda) = 2.303 \cdot e(\lambda)\frac{x}{64500} \tag{5.4}$$

where x is the number of grams of hemoglobin per liter and e(λ) is the molar extinction coefficient. A typical value of x for whole blood is x=150 g Hb/liter [5].

5.4 Erythema Index

To define the skin erythema Dawson's erythema index was used. It is a parameter proportional to the area under the hemoglobin absorption curve, when a baseline is drawn between 510 nm and 610 nm [63]. For the needs of this project the curve of the apparent skin absorption spectra was used, this is described in section 5.5. The erythema index is calculated as:

$$E = [(\mu_a(560) + 1.5\,(\mu_a(540) + \mu_a(575)) - 2\,(\mu_a(510) + \mu_a(610))] \cdot 100\% \tag{5.5}$$

5.5 From Reflectance to Absorbtion

The skin is illuminated with white light and the spectrometer measures the reflected light. The light is divided into spectral components by a diffraction grating and detected by a CCD array. To eliminate the influence of the instrumentation, reflectance from the skin is compared to reflectance from a white standard. The resultant spectra obtained is therefore a relative reflectance. The quantity of apparent absorption, or Log Inverse Reflectance (LIR), refers to the amount of light not returned from the skin, and includes the light which was absorbed in the tissue as well as scattered out of the probe's aperture.

This is calculated by applying an inverse logarithm (equation 5.6) and the result is expressed in Absorption Units [au] [64]:

$$Apparent\ Absorbance = \frac{1}{\log_{10}(Relative\ Reflectance)} \tag{5.6}$$

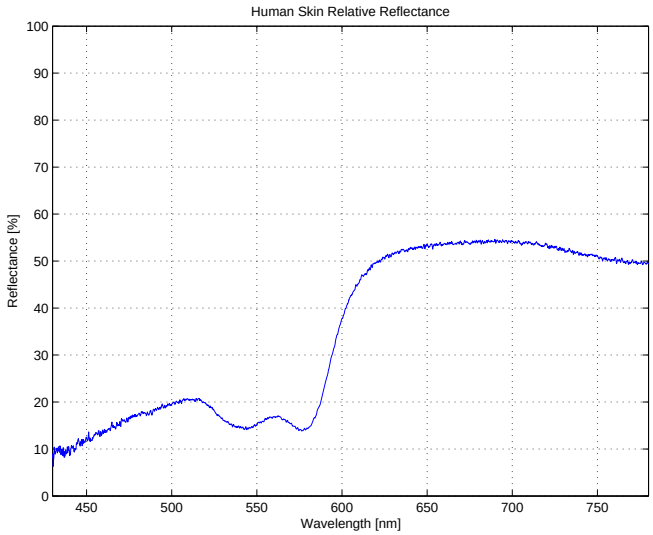

FIGURE 5.3: The relative reflectance of a Caucasian human skin

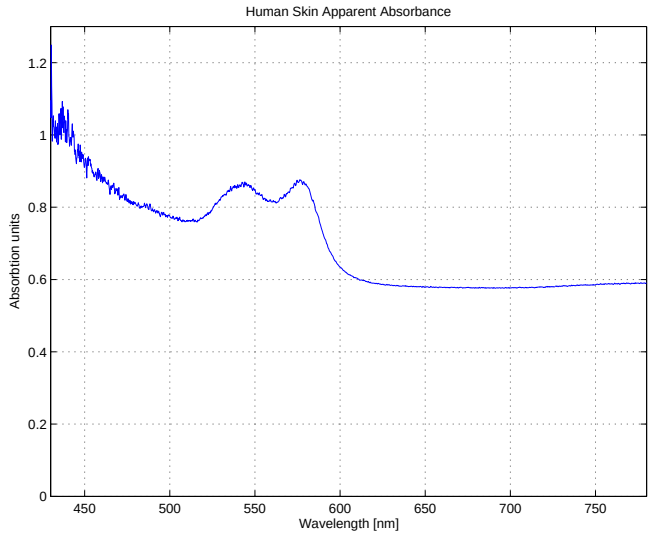

FIGURE 5.4: The apparent absorption spectrum of Caucasian human skin from figure 5.3.

6

Inverse Model

One of the requirements to evaluate the changes between successive skin spectra more effectively than by manual, graphical measurements is to be able to describe the patients spectra with numerical analytical values. To do this an inverse model was developed. The inverse model uses the diffuse skin model to simulate spectra of the same shape as the measured spectra, providing us with the input parameters for the diffuse model. Three input parameters of melanin absorption coefficient, oxygenation and blood volume in the second model layer from section 4.1, together with indices described in section 5 then form a group of seven numbers which are assumed to sufficiently classify and discriminate between the individual measured spectra and to show progression of the skin changes. Although betacarotene can influence the spectra even in small concentrations as demonstrated in section 4.1, it was not used as a relevant parameter in our study. The main reason is that the amount of betacarotene in the subject skin is dependent on dietary habits and does not reflect any changes the skin exhibits when exposed to sun radiation.

The inverse model was realized in the form of a pre-calculated look-up table containing spectra for all the combinations of varied parameters, combined with successive iteration to converge on a more refined solution. The iteration start point is in the middle of the parameters chosen from the look-up table and one previous parameter value. The stop point is in the middle between the chosen look - up element and the following parameter value. The iteration step is one tenth of the look-up table parameter steps. The initial step in the form of the precalculated look-up table was chosen to save calculation time.

The parameter values were swept in the following ranges in the lookup table:

- oxygenation in the second layer of the model from 10% to 90% with three percent step
- melanin absorption coefficient 50 to 1200 m^{-1} with 30 m^{-1} steps
- blood volume in the second layer 0.1% to 10% with 0.15% steps

To determine which of the curves simulated by the diffuse skin model is the best fit to the measured spectra, two approaches were used. The first method was the mean square method, while the second employed the comparison of the indexes described in section 5 together with the mean square method. These were calculated for all possible combinations of varying parameters and for the measured currently compared spectrum. The modeled spectrum with the minimal deviation was chosen and plotted together with the measured spectrum.

7

Spectrometer Setup

7.1 Spectrometer

The spectrometer used for the skin measurements in this project is the Ocean Optics USB4000 Spectrometer [6] equipped with Toshiba TCD1304AP linear array CCD detector with 3648 pixels. This spectrometer is responsive in wavelength range of 200-1100 nm, but specific range and resolution depends on the grating and entrance slit. The equipped grating is tuned to 200 - 850 nm, with an optical bench entrance aperture of 100 μm width. The wavelength resolution is of 0.18 nm

FIGURE 7.1: USB4000 Spectrometer [6].

7.2 Spectrometer Working Principle

This type of spectrometer does not have any moving parts which makes it very robust and convenient for use in the field. The light collected by the integrating sphere enters the spectrometer through an optical fiber. The light then hits the collimating mirror which reflects it onto the grating. The grating diffracts and directs the light onto the focusing mirror. Different gratings allow specific wavelengths and resolutions. The focusing mirror then focuses first - order spectra onto the CCD detector. The detector converts the optical signal into a digital format, with each pixel corresponding to one wavelength band. This digital signal is then transmitted into the computer application through an USB port. The spectrometer internal layout is illustrated on figure 7.2.

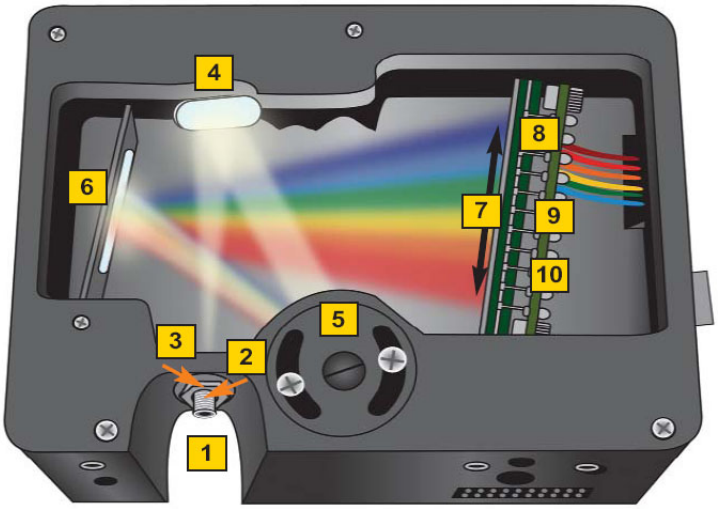

FIGURE 7.2: Internal layout of the USB4000 spectrometer [7]. Where 1) is the connector, 2) the entrance slit, 3) the longpass absorbing filter, 4) the collimating mirror, 5) the grating and wavelength range, 6) the focusing mirror, 7) the detector collection lens, 8) the detector.

7.3 Integrating Sphere

The above desribed spectrometer was used in combination with an Ocean Optics ISP-REF Integrating Sphere designed for even surface illumination for reflectance measurements.

FIGURE 7.3: Ocean Optics ISP-REF Integrating Sphere [7].

This integrating sphere is 1.5” in diameter with a 0.4” aperture and a tungsten-halogen light source with 12 VDC adapter. The spectral range of the illumination source is 360-1000 nm. The sphere is coated with Spectralon, a white diffusing material that provides a highly Lambertian reflecting surface (the surface luminance is isotropic). A simple me-

chanical switch allows users to adjust the sampling optic to include (I) or exclude (E) the specular reflectance [6]. It is possible to measure the surface gloss by calculating the difference between the values with and without specular reflection.

The ISP-REF Integrating Sphere features SMA 905 connectors for two optical fibers, one to be connected to the spectrometer marked “S” (for Sample) and another marked “R” (for Reference). The “R” port can be used as a second channel from the integrating sphere, for example to monitor the built in lamp as a reference for calibration.

7.4 Calibration

For calibration of the setup a Labsphere WS-1-SL White Diffuse Reflectance Standard made of Spectralon was used. Spectralon is a hydrophobic and thermally stable (to 350 °C) material. The Spectralon material (doped with Barium Sulfate) used for the standard has reflectivity >98% (400-1500 nm) and >95% (250-2000 nm) [6]. The same material is used for coating of the integrating sphere.

FIGURE 7.4: WS-1-SL White Diffuse Reflectance Standard [7].

8

Preparations for Practical Measurements

To successfully finish the experimental survey of patients skin several practical preparations have to be done on site in the climate therapy center and can not be carried out beforehand. These include for example setup of the room (including bed or chair for the patients) or preparation of a steady holder for the spectrometer fiber probe. The preparations that were possible to be carried out beforehand are summarized in the following sections.

8.1 UV Dosimetry

A common technique to measure patient UV doses is to employ personal dosimeters. Normally, people do not maintain a fixed position with respect to the UV radiation source, and so measurements using a stationary detector can be of limited value. Personal dosimeters usually consist of a photosensitive film where the UV induced deterioration of the film is calibrated to the measured UV irradiance. A commonly employed film dosimeter material is the polysulphone polymer, popular because it is robust and due to its low cost. Personal UV detectors in form of wrist watches can give valuable extra information, but are much more expensive.

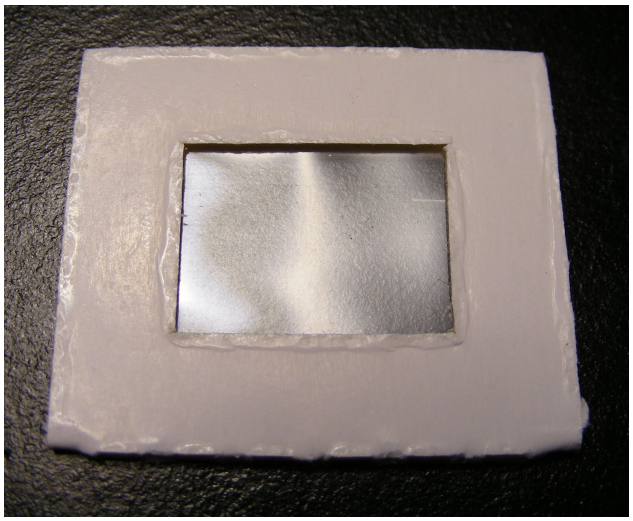

FIGURE 8.1: Original polysulphone film dosimeter.

A practical personal dosimeter for UV radiation is a polysulphone film, which after exposure to ultraviolet radiation in the spectral range 250 to 330 nm shows an increase in absorbance at 330 nm. Polysulphone film has a spectral response (CIE 98-1992) that approximates the erythemal response of human skin (CIE S007/E-1999).

This film employed in dosimeters is of approximate size 3 cm x 3 cm and allows the monitoring of personal UV exposures during normal daily activities to determine the personal UV dose of the psoriasis patients. The polysulphone film of the selected personal dosimeter is attached in a cardboard holder as shown in figure 8.1, which may be potentially impractical for the use on climate therapy patients as discussed in section 9.3.

Variations in film thickness may occur during the film casting process and introduce significant variations in the dose response of the film. Each badge therefore undergoes a unique calibration and it is important that the unique id for each badge is retained from initial calibration to final reading of the badge.

Part III

Results, Discussion and Conclusion

9

Results

9.1 Inverse Model Performance

The proposed inverse model algorithm was tested on several different normal non-psoriatic skin spectra. These are a completely anonymous set of data, collected through research by Lill T. N. Nilsen [10].

The measured spectra can be described by three numbers generated from the inverse model algorithm based on the measured spectra fitting. These are the diffuse skin model input parameters determined to be most relevant for the observation of skin changes caused by sun exposure and should describe the properties of the measured skin. These numbers are oxygenation in the second model layer (Oxy2), blood volume in the second model layer (BV2) and melanin absorption coefficient at 694 nm in $[m^{-1}]$ (Mel_{694}).

Furthermore, melanin index, hemoglobin index, oxygenation index and erythema index were suggested for the evaluation of the skin properties and calculated. The mentioned indexes were obtained with the use of formulas detailed in section 5, which were applied on the original measured spectra.

Every spectrum used for the model testing is plotted together with the modeled spectra curves. Two approaches were used and visually compared, the first (drawn in blue color on the graphics) is based only on minimizing the mean square difference between the model and the measured spectrum. The second approach considers the mean square difference and compares the indexes calculated for both model and measured spectra and searches for minimal difference of these five fitting parameters.

The acquired numbers describing the skin properties are stated under the spectra figures, the percentages of Oxy2 and BV2 and all the indexes in the results are expressed in their decimal number form. The results found for oxygenation in the second model layer in the table are presented with the precision of two decimal places since the step for the inverse model is in the size of units of percents. The results for blood volume in the second model layer are stated in the order of four decimal places since the step in this case for the inverse model is in tenths of percent, and rounding to only two decimal places would lead to a loss of information.

The following figures do not have the same scale on y-axis since the comparison of the measured and simulated spectra in more detail is here more relevant than comparisons between individual skin spectra.

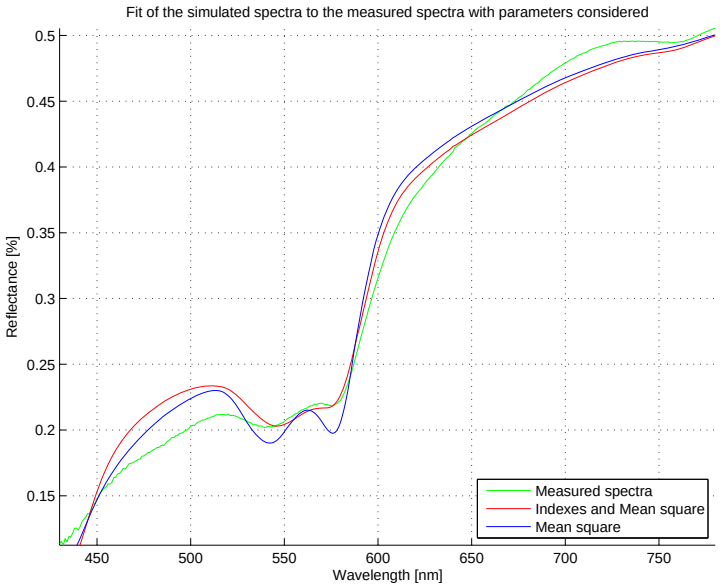

FIGURE 9.1: Test spectra A fitted by two model approaches

Oxy2	**BV2**	$\mathbf{Mel_{694}}$	**Oxygenation index**	**Melanin index**	**Hemoglobin index**	**Erythema index**
0.10	0.034	830	0.88	1.88	0.11	21.21

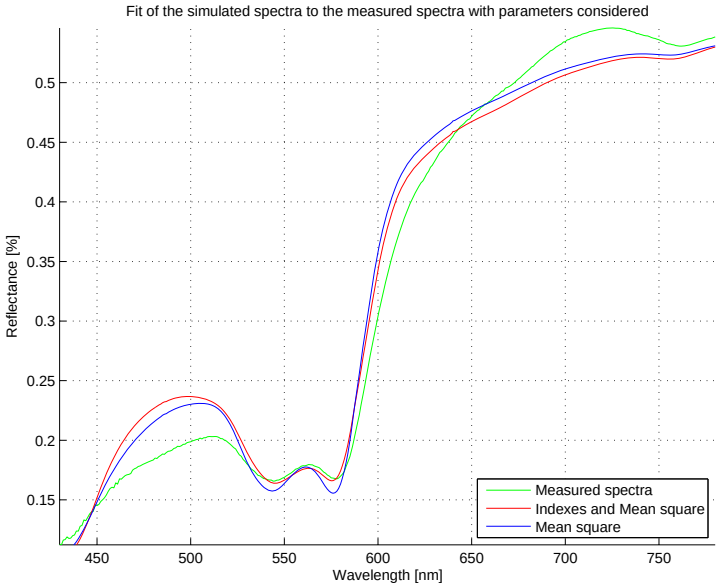

FIGURE 9.2: Test spectra B fitted by two model approaches

Oxy2	**BV2**	$\mathbf{Mel_{694}}$	**Oxygenation index**	**Melanin index**	**Hemoglobin index**	**Erythema index**
0.10	0.01	290	0.84	0.62	0.07	13.55

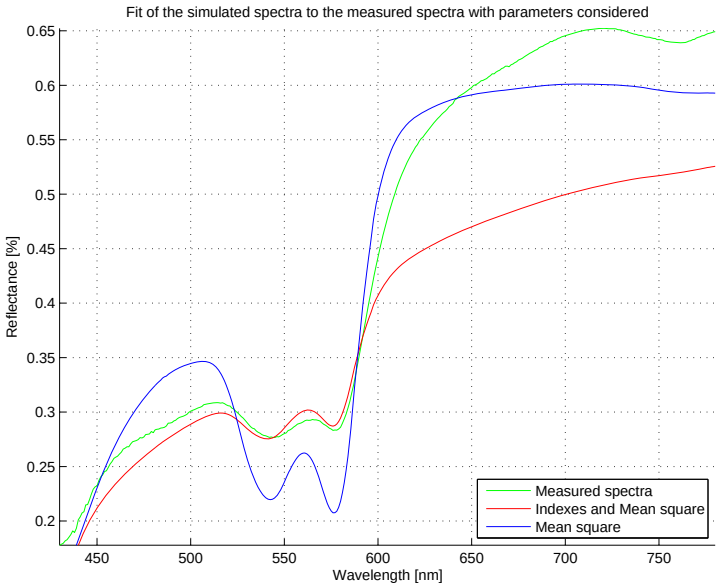

FIGURE 9.3: Test spectra C fitted by two model approaches

Oxy2	**BV2**	$\mathbf{Mel_{694}}$	**Oxygenation index**	**Melanin index**	**Hemoglobin index**	**Erythema index**
0.60	0.005	650	0.85	1.02	0.10	23.85

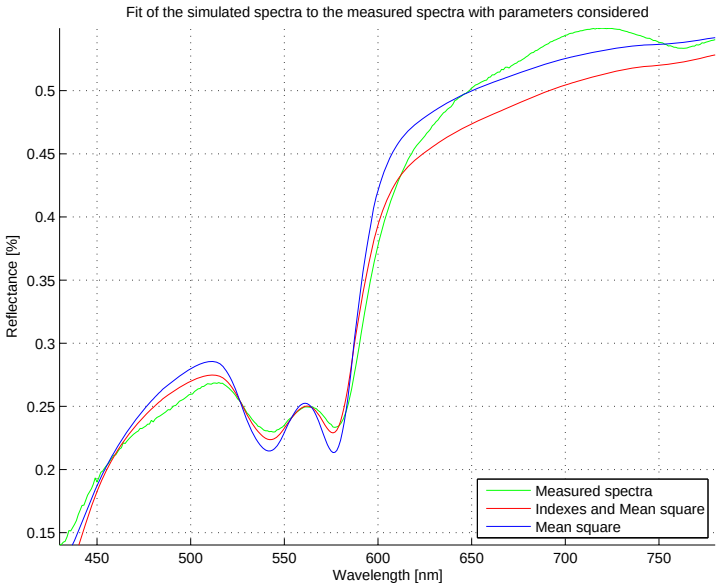

FIGURE 9.4: Test spectra D fitted by two model approaches

Oxy2	**BV2**	$\mathbf{Mel_{694}}$	**Oxygenation index**	**Melanin index**	**Hemoglobin index**	**Erythema index**
0.60	0.03	600	0.88	1.17	0.16	28.48

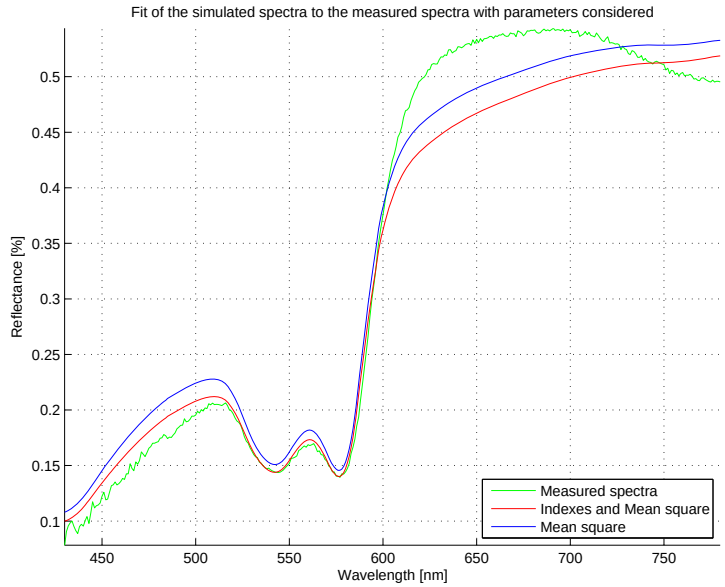

FIGURE 9.5: Test spectra E fitted by two model approaches

Oxy2	**BV2**	$\mathbf{Mel_{694}}$	**Oxygenation index**	**Melanin index**	**Hemoglobin index**	**Erythema index**
0.85	0.10	600	0.93	0.20	0.33	68.66

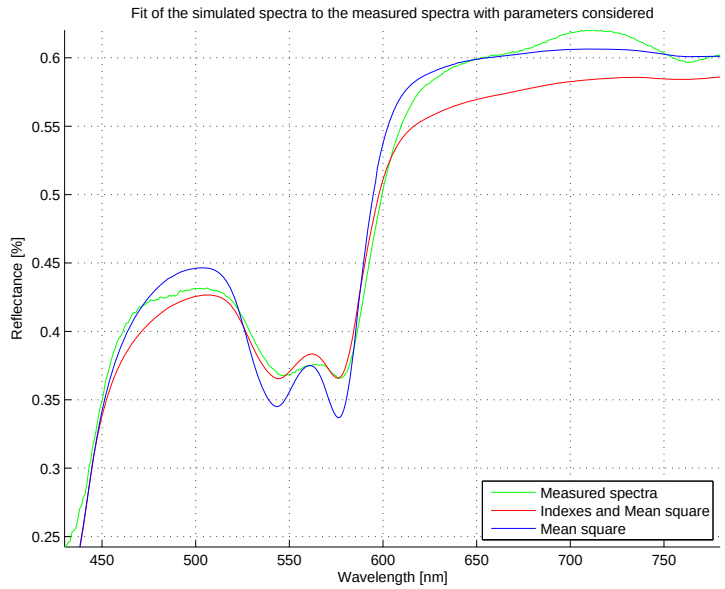

FIGURE 9.6: Test spectra F fitted by two model approaches

Oxy2	**BV2**	$\mathbf{Mel_{694}}$	**Oxygenation index**	**Melanin index**	**Hemoglobin index**	**Erythema index**
0.10	0.006	250	0.81	0.42	0.10	17.84

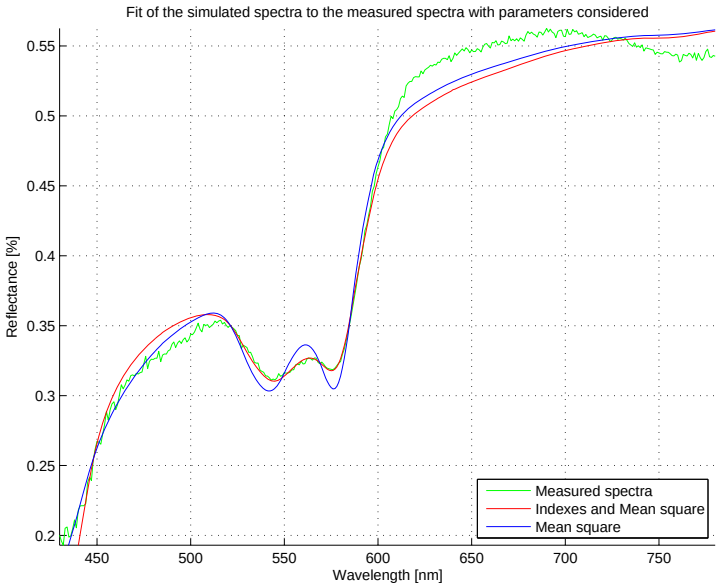

FIGURE 9.7: Test spectra G fitted by two model approaches

Oxy2	**BV2**	$\mathbf{Mel_{694}}$	**Oxygenation index**	**Melanin index**	**Hemoglobin index**	**Erythema index**
0.10	0.011	400	0.85	0.27	0.09	19.44

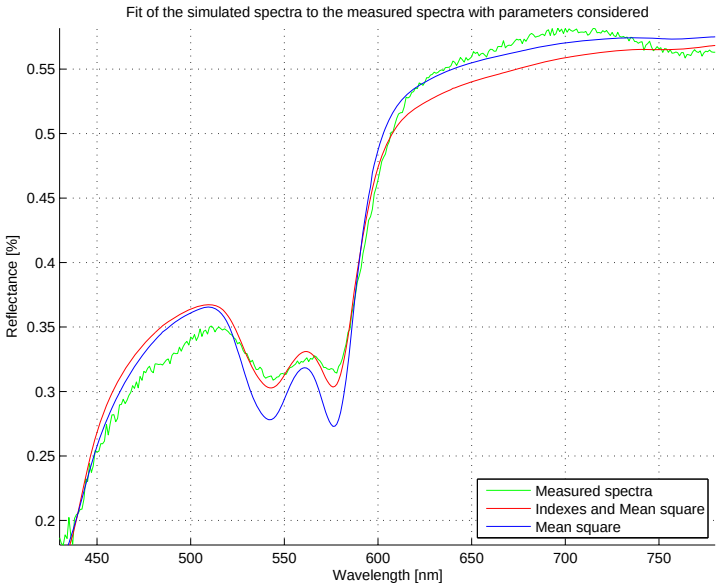

FIGURE 9.8: Test spectra H fitted by two model approaches

Oxy2	**BV2**	$\mathbf{Mel_{694}}$	**Oxygenation index**	**Melanin index**	**Hemoglobin index**	**Erythema index**
0.60	0.015	350	0.86	0.49	0.11	19.98

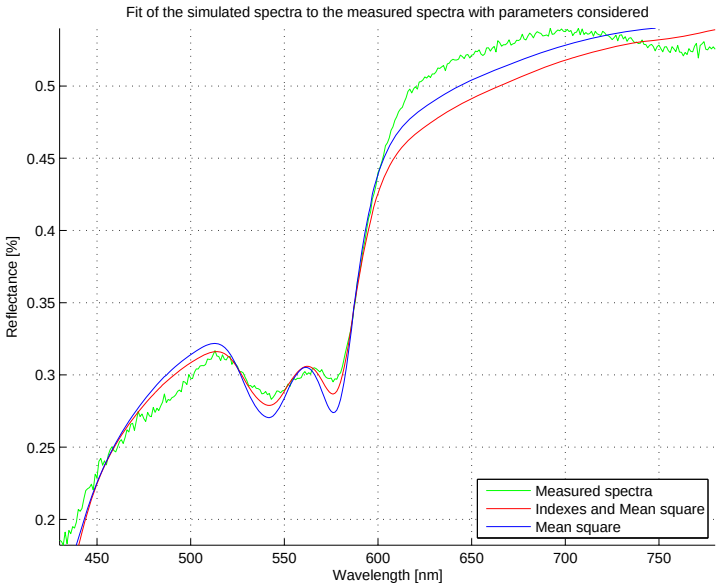

FIGURE 9.9: Test spectra I fitted by two model approaches

Oxy2	**BV2**	$\mathbf{Mel_{694}}$	**Oxygenation index**	**Melanin index**	**Hemoglobin index**	**Erythema index**
0.60	0.010	550	0.84	0.44	0.10	19.91

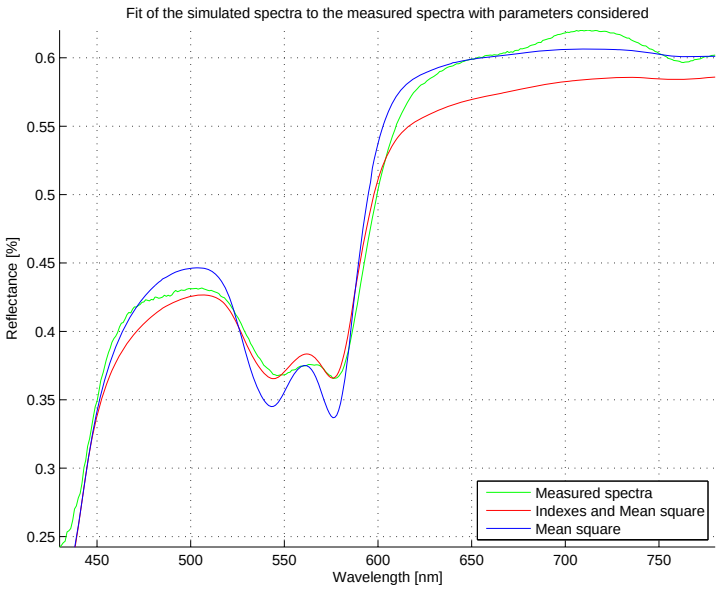

FIGURE 9.10: Test spectra J fitted by two model approaches

Oxy2	**BV2**	$\mathbf{Mel_{694}}$	**Oxygenation index**	**Melanin index**	**Hemoglobin index**	**Erythema index**
0.10	0.011	400	0.82	0.54	0.09	16.68

9.2 Psoriasis Spectra Fitting

To test the inverse model performance also with connection to psoriasis spectra, in the absence of the formerly planned survey amongst the climate therapy patients, spectra from one volunteer were measured. These spectra were measured on the psoriatic plaques on the leg and arm of the volunteer, which can be seen on the photographs in figures 9.11a and 9.11b respectively. A healthy skin sample spectrum was also measured next to each of the plaques. To assess the possible effects of hairs on the spectroscopic measurements, the measurements were carried for both shaven and unshaven skin on both leg and arm for healthy and psoriatic skin. Each measured spectrum is plotted with two inverse model fitted modeled spectra as in section 9.1 and a table under the figures gives the indexes calculated for the measured spectra and the parameters found through the inverse model fitting, as described in section 9.1.

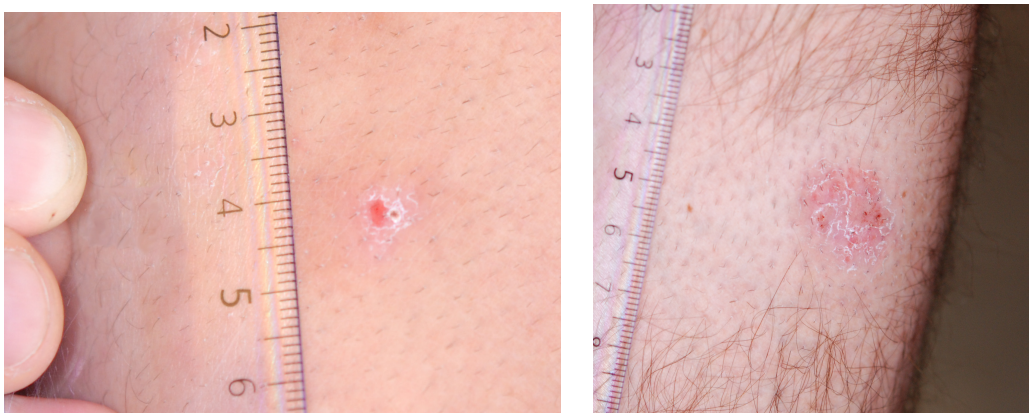

(a) Psoriasis plague A on the arm of the volunteer

(b) Psoriasis plague B on the leg of the volunteer

FIGURE 9.11: Measurements volunteer psoriasis.

The following figures do not have the same scale on y-axis since the comparison of the measured and simulated spectra in more detail is here more relevant than comparing the single skin spectra between each other. Since comparing the normal skin spectra and psoriatic skin spectra of the same subject is of interest, these are plotted in one figure with the same scale on y-axis in a later section in the figure 10.1.

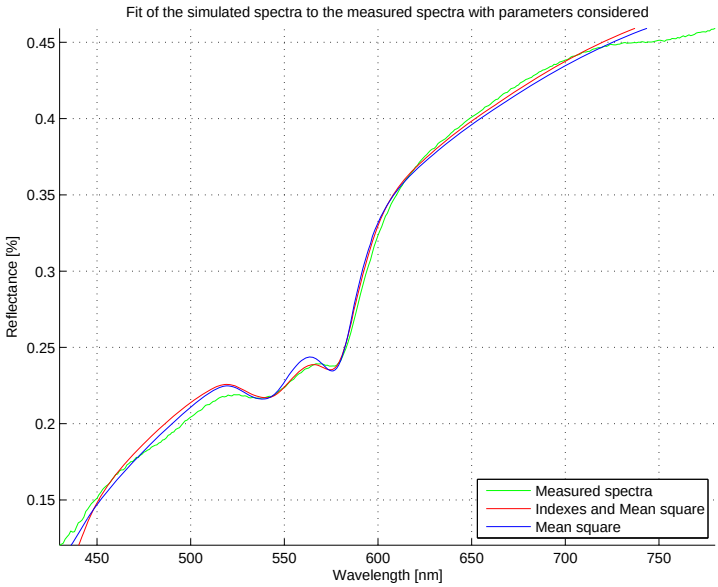

FIGURE 9.12: Volunteer spectrum of normal skin on the arm before shaving, fitted by two model approaches

Oxy2	**BV2**	$\mathbf{Mel_{694}}$	**Oxygenation index**	**Melanin index**	**Hemoglobin index**	**Erythema index**
0.1	0.007	1010	0.90	1.47	0.07	13.87

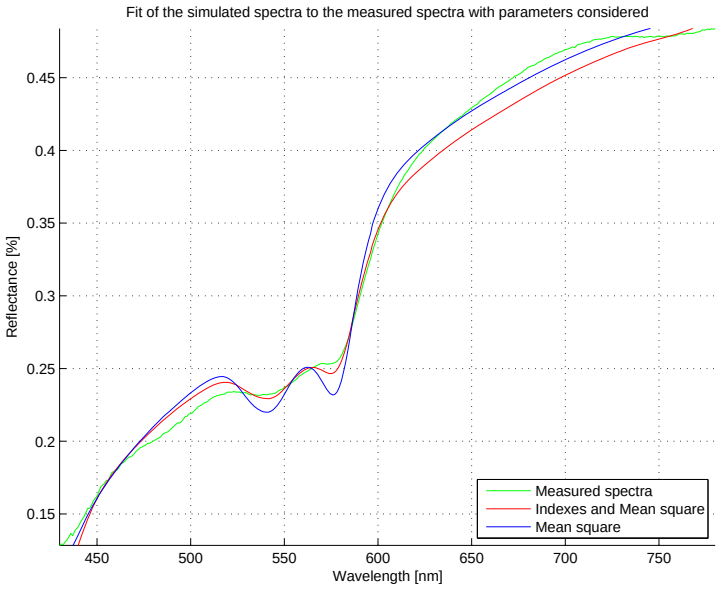

FIGURE 9.13: Volunteer spectrum of normal skin on the arm after shaving, fitted by two model approaches

Oxy2	**BV2**	$\mathbf{Mel_{694}}$	**Oxygenation index**	**Melanin index**	**Hemoglobin index**	**Erythema index**
0.10	0.007	920	0.88	1.41	0.06	14.03

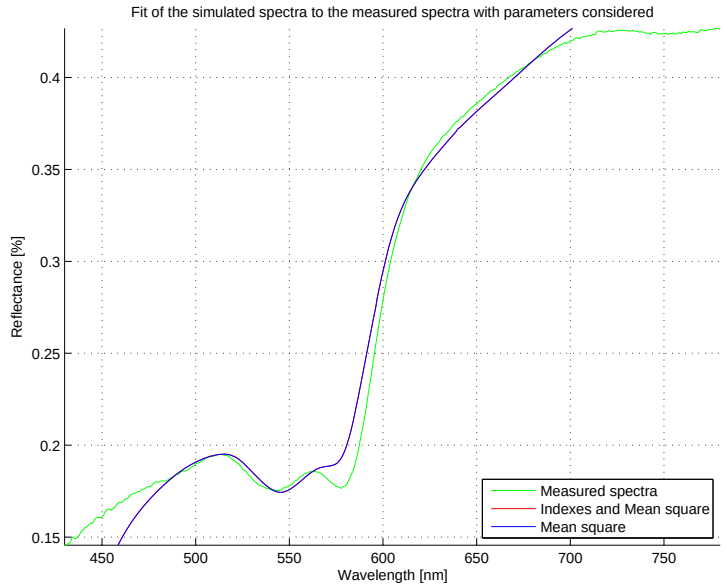

FIGURE 9.14: Volunteer spectrum of psoriatic skin on the arm before shaving, fitted by two model approaches

Oxy2	**BV2**	$\mathbf{Mel_{694}}$	**Oxygenation index**	**Melanin index**	**Hemoglobin index**	**Erythema index**
0.1	0.034	1040	0.84	1.42	0.11	31.93

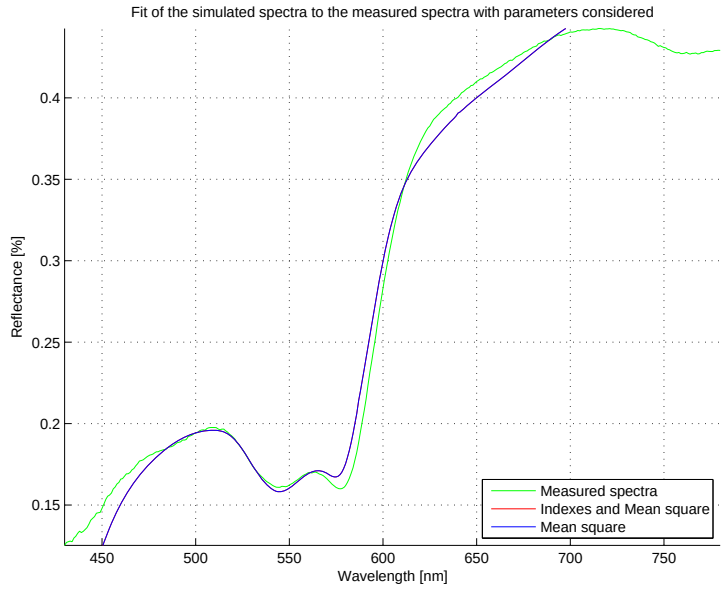

FIGURE 9.15: Volunteer spectrum of psoriatic skin on the arm after shaving, fitted by two model approaches

Oxy2	**BV2**	$\mathbf{Mel_{694}}$	**Oxygenation index**	**Melanin index**	**Hemoglobin index**	**Erythema index**
0.31	0.061	890	0.83	1.16	0.21	45.22

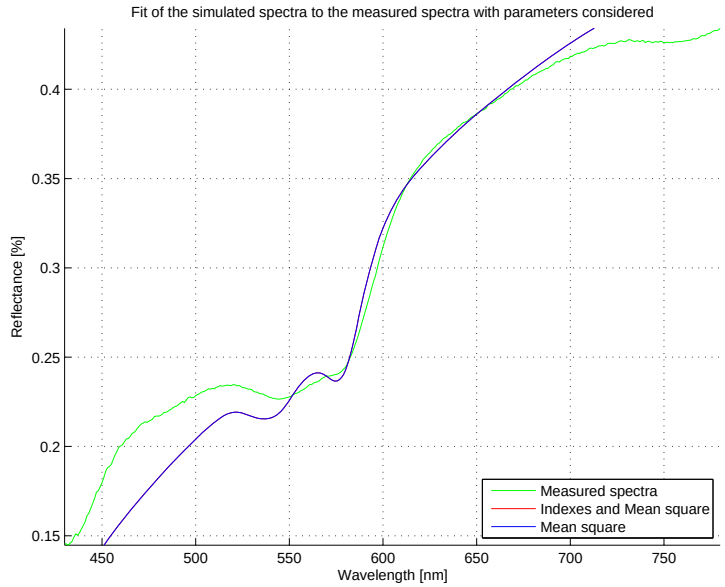

FIGURE 9.16: Volunteer spectrum of normal skin on the leg before shaving, fitted by two model approaches

Oxy2	**BV2**	$\mathbf{Mel_{694}}$	**Oxygenation index**	**Melanin index**	**Hemoglobin index**	**Erythema index**
0.1	0.001	1100	0.84	1.35	0.08	15.34

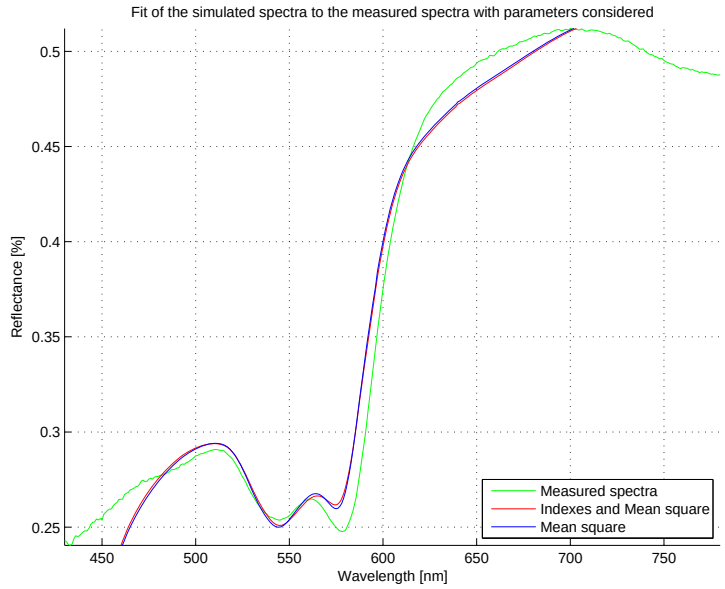

FIGURE 9.17: Volunteer spectrum of normal skin on the leg after shaving, fitted by two model approaches

Oxy2	**BV2**	$\mathbf{Mel_{694}}$	**Oxygenation index**	**Melanin index**	**Hemoglobin index**	**Erythema index**
0.16	0.022	560	0.84	0.54	0.09	25.35

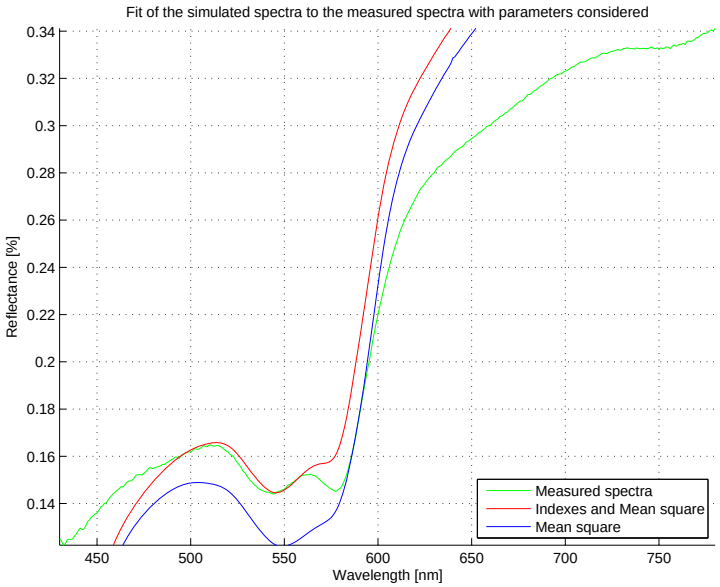

FIGURE 9.18: Volunteer spectrum of psoriatic skin on the leg before shaving, fitted by two model approaches

Oxy2	**BV2**	**Mel_{694}**	**Oxygenation index**	**Melanin index**	**Hemoglobin index**	**Erythema index**
0.16	0.052	1190	0.86	1.83	0.16	35.61

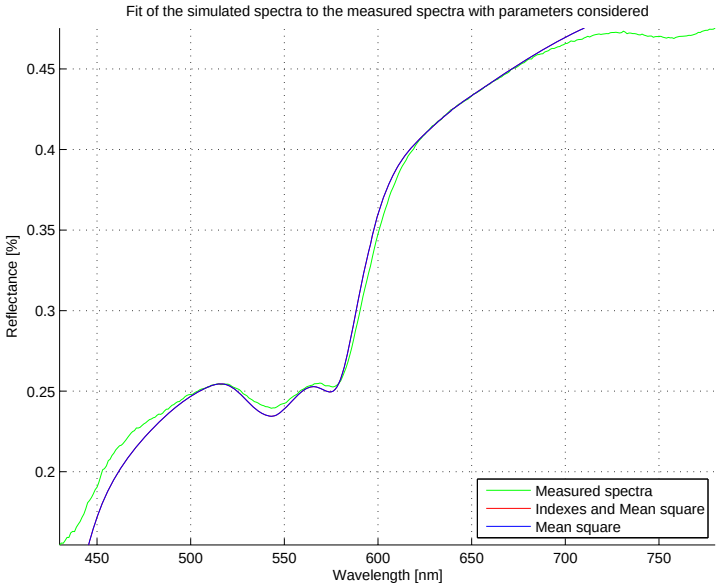

FIGURE 9.19: Volunteer spectrum of psoriatic skin on the leg after shaving, fitted by two model approaches

Oxy2	**BV2**	**Mel_{694}**	**Oxygenation index**	**Melanin index**	**Hemoglobin index**	**Erythema index**
0.1	0.013	800	0.87	1.14	0.09	18.14

9.3 Personal Dosimeters

The question asked regarding the ordered dosimeters was: Can this dosimeter stand the rigors of swimming in the sea and the pool and all other activities (towel rubbing, being leant on on the beach) throughout one day? The dosimeter was subjected to about two hours of testing involving salt water, fresh water, drying and light rubbing. The result of this test can be seen on figure 9.20 where most of the cardboard frame detached. This tested dosimeter was submitted to further and analysis and it has been found that the polysulphone film reaches several millimeters into the cardboard holder, namely 3 millimeters on the longer axis and 4 millimeters on the shorter axis, as can be seen on figure 9.21. The first technique considered for attaching the dosimeters to patients' bathers was with the use of safety pins.

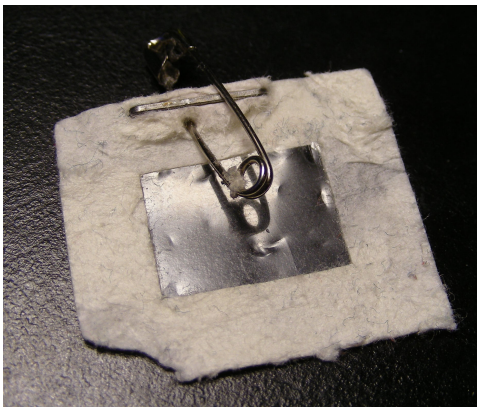

FIGURE 9.20: Polysulphone film dosimeter after salt water and tap water test.

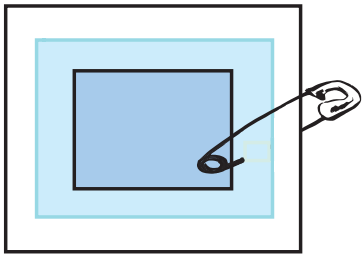

FIGURE 9.21: Polysulphone film scheme.

10

Discussion

10.1 Spectra Fitting

This discussion section is dedicated to the evaluation of the inverse model performance regarding fitting of the normal skin measured spectra. This performance was evaluated visually. Visual evaluation is in this case preferred over for example evaluation with deviation because the model can perform well at some parts of the spectra while having a very bad fit at other less relevant parts of the spectra. Also each part of the spectra is influenced with different factors as suggested in section 2.1.3 and some of these (such as betacaroten levels) are completely unrelated to the sun exposure caused skin changes.

First the performance of the two approaches (that were chosen for minimization of the deviation between the measured and simulated spectra to find the best fit) will be evaluated. For normal skin spectra results (from section 9.1) the approach that was minimizing also the skin parameters performed better than the one considering only the mean square difference of the whole spectra. This was an expected result since the parameters give the model the possibility to compare the parts of the spectra which are relevant for the skin qualities we are interested in. Therefore the risk of an error originating from trying only to find the compromise on the whole length of the spectra and thereby neglecting the melanin slope or hemoglobin-oxygenation peaks is much lower.

When looking at simulated spectra from the better performing approach only there are some regions of the spectra where the diffuse skin model in the combination with the inverse model has higher deviation. These are the lower wavelengths up to approximately 530 nm and the further part of the spectra from about 600 nm.

The mismatch of the lower part of the spectra can be explained with the lack of betacaroten consideration in the inverse model. The reason for this is the fact that betacaroten is not relevant for determining the sun exposure caused skin changes. Other factor can be varying scattering due to for example higher age which causes the loss of collagen in the skin and lowers the scattering for lower wavelengths (described in section 2.3.3.1) as can be seen in the result spectra. Since these spectra are completely anonymous there is no way how to determine the age of the subject. In further work these factors could be corrected on an individual basis by measuring both sun exposed and unexposed skin. This deviation can be also explained by violation of the assumption $\mu_s \gg \mu_a$ for the diffusion approximation equation 2.29.

The deviation at the end of the spectrum can be attributed to water absorption which is not included in the model. The underestimation of the measured model by the spectra between 600 nm and 700 nm which can be seen in the figures 9.7 and 9.9 can be explained by omitting several other constituents of the skin either because of their irrelevance or because they are not included in the model as in the work of [65], where a similar task was challenged. For practical use the fitting of the model can be further improved by the use of smaller steps in the generated lookup table and by considering scattering in the different layers or layers' thicknesses among the varying parameters.

10.2 Psoriatic Plaques Spectra

In this section the results of the psoriatic plaques spectra from chapter 9.2 measured together with normal skin on the volunteer are discussed. The spectra of the normal skin show the same model fitting performance as those in section 10.1, these are namely on figures 9.12, 9.13, 9.16, 9.17. Again the approach considering the skin parameters together with the mean square difference between the measured and fitted spectra performs better than the one considering only the mean square method. The spectra taken before shaving shows increased pigmentation compared with the spectra after shaving, which can be explained by the hair pigment contributing while taking the measurements with the integrating sphere which has quite a wide aperture.

The psoriatic spectra on figures 9.14, 9.15, 9.18 and 9.19 seem to be approximated by the two considered approaches with the same precision and their curves lie on top of each other. The deviance of the model in the beginning of the spectra up to 500 nm can also be explained by increased scattering caused by the psoriatic scales in the plaques.

The spectra can be compared on the same scale in the same plot in figure 10.1. The psoriatic plaques demonstrate lower reflectance on average except one measured on the volunteers leg after shaving which can be explained by increased blood volume and scattering. Climate and UV treatment slows down the process of skin cell development and skin scattering and skin thickness is expected to be reduced after the treatment. Hence for further improvement of the model efficiency on psoriatic skin scattering and thickness should be included as a varying parameter in the model.

10.3 Personal Dosimeters

The dosimeter is not able to withstand the rough conditions on the beach and around pool in the original form, but if we attach the safety pin correctly we can assure not to lose the polysulphone film. However this solution is not sufficient since the cardboard holder plays an important role in the calibration and the evaluation of the badge. Other methods like covering the cardboard in polish or plastic case should be considered; it could be advantageous to base this solution on analyzing the position of the actually measured area, since the rest of the badge can be covered as illustrated on figure 10.2.

A method of retaining the unique id for each badge must be used during handout and return of badges. The badges will be given to the patients in pairs and each of them should have unique number for easy identification which will match the badge's unique id in a database. These numbers can be noted on the patients' form each morning when the badges are distributed.

10.4 Patients Data and Other Data Handling

The output data from the spectrometer are saved in .txt format for easy access and processing. To ensure the correct tracking of each measurement that was done to the correct patient, date, time of day and body site, the data files of each patient must be saved under a uniform and thoughtfully designed naming scheme. It has been decided that the safest way is to encode all the information in easily readable and sortable way directly in the file name. This way the files can be handled without any other additional information or key. The file naming system is illustrated on table 10.1.

Patient	Measurement	Skin/Lesion	Body site	Date	Hour
A, B, C, D, ...	1, 2, 3, 4,...	S / L	A, B, C, ...	316, 317, ...	942, 943, ...

TABLE 10.1: Table illustrating the naming system of files containing measured spectra.

To keep track of the patients prior sun exposure and habits which may possibly influence the skin condition a form will be filled with every patient involved, also including the age, gender and hair color which may have relation to the skin type and skin color . This form asks about coffee and cigarettes consumption since the latter cause contractions of the blood vessels in the skin, about the use of skin creams which can change the measurements and physical activity which may increase the blood volume in the skin. It will also help to keep track of the patients measurements, dosimeters and the conditions during the measurements (room temperature). These forms will be later used to exclude the variations in the measurements caused by aforementioned factors rather than by sun exposure.

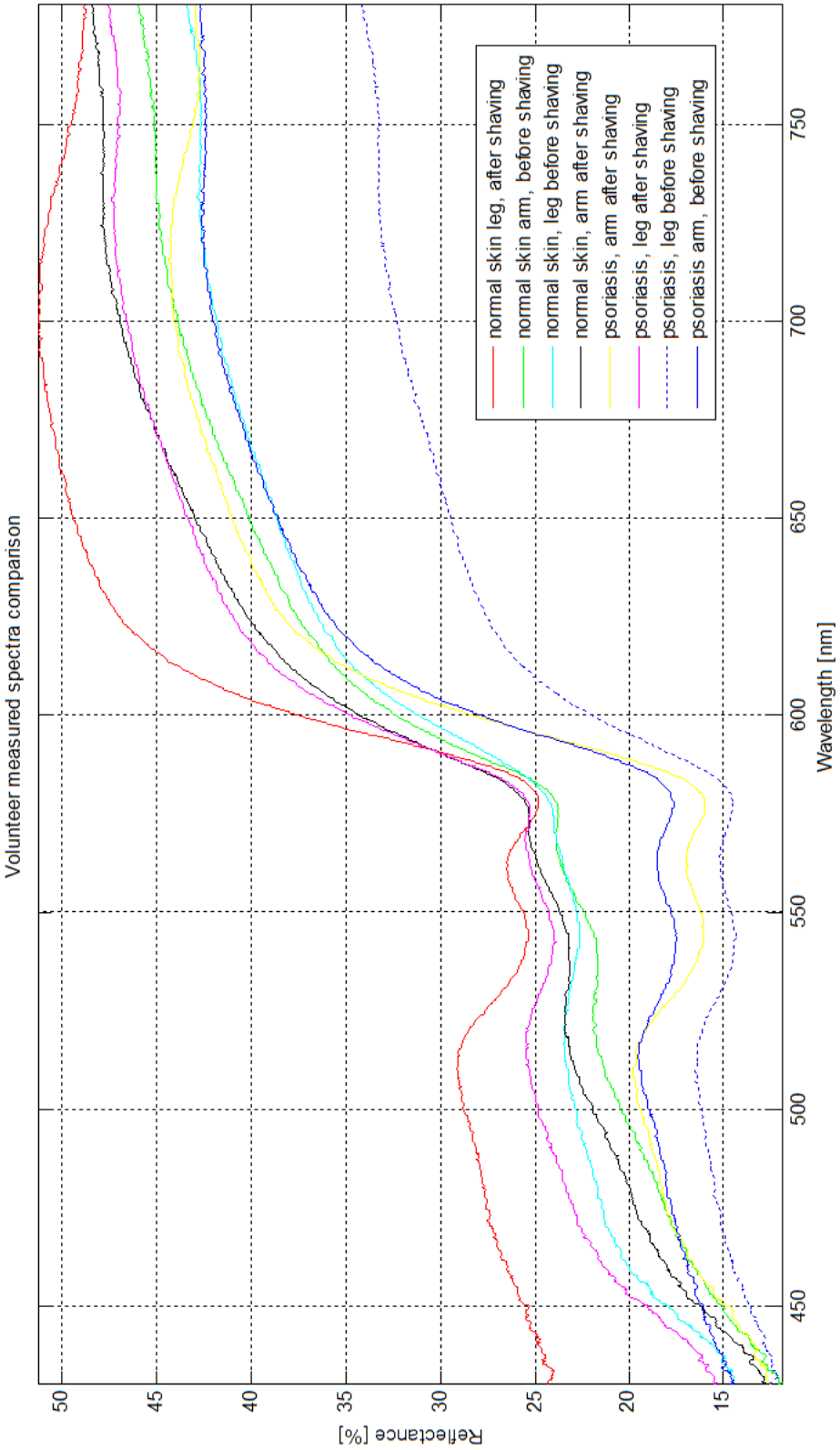

FIGURE 10.1: Volunteers spectra of psoriatic skin and normal skin

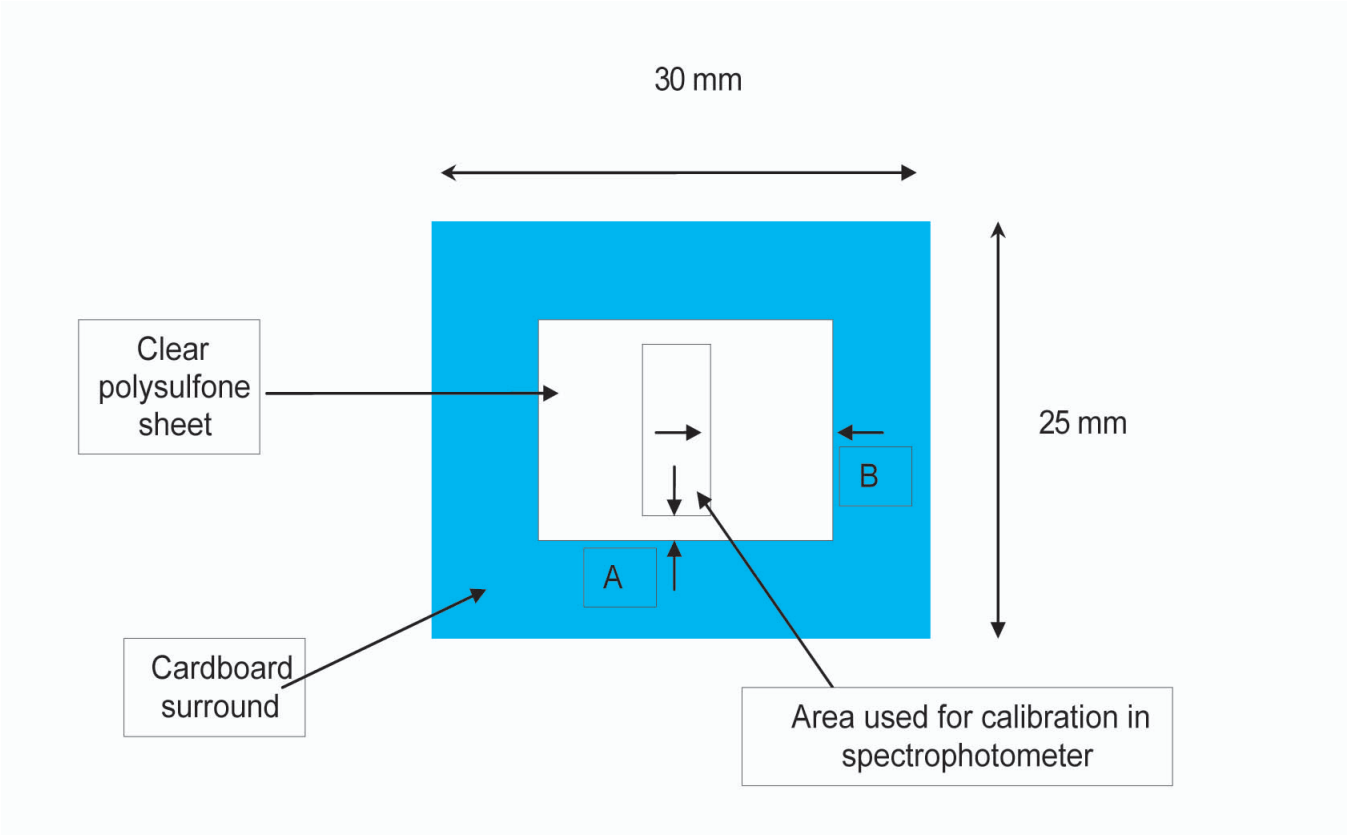

FIGURE 10.2: Polysulphone film scheme. Polysulfone Badge area of clear polysulfone not required for calibration. Distance A = 1 mm, B = 4 mm

11

Conclusions

In this project an inverse model was proposed to find the diffusion skin model input parameters that can be used to describe the skin properties. The inverse model performs quite well while fitting the spectra of normal skin as well as the spectra of the psoriatic plaques. The spectrum chosen as the best fit of the measured spectra is far from perfect match but for the needs of automatic evaluation of large volumes of data without human being interventions this accomplishment might be sufficient. Most frequently the imperfections of the inverse model fitting can be found at the beginning and at the end of the spectra. The spectra matching can be further improved by studying the effects of adding the scattering or skin layer thicknesses to the changing parameters used for the lookup table generation. The diffusion skin model input parameters can then be used together with the four indexes calculated on the measured spectra from section 2.1.3 to evaluate the measured skin spectra and also measured psoriasis skin spectra in future experimental measurements.

When evaluating the study results it is important to take into account the patients' smoking habits, physical activity and other factors which may potentially bias both the measurements outcomes and the treatment effects. The fit of the simulated spectra will never be perfect unless even chromophores and scatterers considered irrelevant for the sun exposure caused changes are added, like for example betacarotene and bilirubin.

Parallel practical preparations were realized in the form of dosimeter endurance testing and suggestions for patient data handling were made. Regarding the dosimeters other preventive steps need to be taken before these can withstand a whole day of patient climate therapy treatment.

12

References

[1] Wikimedia Commons. Skin scheme. http://en.wikipedia.org/wiki/File:Skin.jpg, March 2010.

[2] S. Prahl. Extinction coefficient of melanin. http://omlc.ogi.edu/spectra/melanin/extcoeff.html, March 2010.

[3] S. Prahl. The molar extinction coefficient of beta-carotene. http://omlc.ogi.edu/spectra/PhotochemCAD/html/beta-carotene.html, March 2010.

[4] K. Hanson and J. D. Simon. Epidermal trans-urocanic acid and the UV-A-induced photoaging of the skin. *PNAS*, 95:10576–10578, 1998.

[5] S. Prahl. Tabulated molar extinction coefficient for hemoglobin in water. http://omlc.ogi.edu/spectra/hemoglobin/summary.html, March 2010.

[6] Ocean Optics. *Installation and Operation Manual.* USB4000 Fiber Optic Spectrometer.

[7] Ocean Optics. Spectrometers catalogue. http://www.oceanoptics.com/Products/catalogspectrometers.pdf, March 2010.

[8] V. Bartosova. UV doses to psoriasis patients undergoing climate therapy. NTNU Specialization Project, Trondheim 2009.

[9] L. L. Randeberg. *Diagnostic applications of diffuse reflectance spectroscopy.* Doctoral thesis NTNU, 2005.

[10] L. T. Norvang. *In Vivo Spectroscopy of Human Skin; Characterization of Port-wine Stain.* Doctoral thesis NTNU, 1996.

[11] W. Verkruysse, R. Zhang, B. Choi, G. Lucassen, L. O. Svaasand, and J. S. Nelson. A library based fitting method for visual reflectance spectroscopy of human skin. *Phys. Med. Biol.*, 50:57–70, 2005.

[12] E. N. Marieb and K. Hoehn . *Human anatomy and physiology.* Pearsons Education, 2007.

[13] P. Tate and R. R. Seeley and T. D. Stephens. *Essentials of anatomy and physiology.* McGraw Hill, 2007.

[14] R. Drugge and H. A. Dunn. *The Electronic Textbook of Dermatology*. http://www.telemedicine.org/stamford.htm, 20010.

[15] S. L. Jacques. Skin optics. `http://omlc.ogi.edu/news/jan98/skinoptics.html`, June 2010.

[16] V. J. Hearing and S. P. Leong. *From Melanocytes to Melanoma: The Progression to Malignancy*. Humana Press Inc., 2006.

[17] A. R. Young. Chromophores in human skin. *Phys. Med. Biol.*, 42:789 – 802, 1997.

[18] J. B. Dawson, D. J. Barker, D. J. Ellis, E. Grassam, J. A. Cotterill, G. W. Fisher, and J. W. Feather. A theoretical and experimental study of light absorption and scattering by in vivo skin. *Phys. Med. Biol.*, 25:695–709, 1980.

[19] M. L. Wolbarsht, A. W. Walsh, and G. George. Melanin, a unique biological absorber. *Appl. Opt.*, 20:2184 – 2186, 1981.

[20] H. Du, R. A. Fuh, J. Li, A. Corkan, and J. S. Lindsey. Photochemcad: A computer-aided design and research tool in photochemistry. *J Photochem Photobiol*, 68:141 – 142, 1998.

[21] A. Scott and E. Fong . *Body Structures and Functions*. Delmar Learning, 2003.

[22] N. H. Grynaviski, C. Ransom, K. Hanson, and J. D. Simon. The in vitro photochemistry of urocanic acid. `http://www.photobiology.com/photoiupac2000/grynaviski/urocanic.html`, May 2010.

[23] A. Sleijffers, A. Kammeyer, F. R. de Gruijl, G. J. Boland, J. van Hattum, W. A. van Vloten, H. van Loveren, M. B. Teunissen, and J. Garssen. Epidermal cis-urocanic acid levels correlate with lower specific cellular immune responses after hepatitis b vaccination of ultraviolet b-exposed humans. *Photochem Photobiol*, 77:271–275, 2003.

[24] J. W. Gilmour, J. P. Vestey, S. George, and Mary Norval. Epidermal cis-urocanic acid levels correlate with lower specific cellular immune responses after hepatitis b vaccination of ultraviolet b-exposed humans. *J Invest Dermatol*, 101:169–174, 1993.

[25] A. L. Cameron, B. Kirby, W. Fei, and C. E. M. Griffiths. Natural killer and natural killer-t cells in psoriasis. *Arch Dermatol Res*, 294:363–369, 2002.

[26] S. Astner and R. R. Anderson. Skin phototypes 2003. *J Invest Dermatol*, 122, 2004.

[27] S. Franceschi, F. Levi, L. Randimbison, and C. La Vecchia. Site distribution of different types of skin cancer: new aetiological clues. *International Journal of Cancer*, 67(1):24–28, 1998.

[28] B. K. Armstrong and A. Kricker. The epidemiology of UV induced skin cancer. *Journal of Photochemistry and Photobiology B: Biology*, 63:8–18, 2001.

[29] A. Osmancevic. *Vitamin* D *status in psoriasis patients treated with* UVB *therapy*. Intitute of Clinical Sciences at Sahlgrenska Academy, University of Gotheburg, 2006.

[30] K. S. Kochanek, P. Brenneisena, J. Wenka, G. Herrmanna, W. Maa, L. Kuhra, C. Meewesa, and M. Wlascheka. Photoaging of the skin from phenotype to mechanisms. *Experimental Gerontology*, 35:307–316, 2000.

[31] H. Sies. Oxidative stress: oxidants and antioxidants. *Experimental Physiology*, 82:291, 1997.

[32] B. N. Ames, M. K. Shigenaga, and T. M. Hagen. Oxidants, antioxidants, and the degenerative diseases of aging. *Proceedings of the National Academy of Sciences*, 90:7915, 1993.

[33] M. N. O. Sadiku. *Elements of Electromagnetics*. Oxford University Press, 2001.

[34] A. K. Pahari and B.S. Chauhan . *Engineering Chemistry*. Laxmi Publications, 2006.

[35] B. A. E. Saleh and M. C. Teich. *Fundamentals of photonics*. Wiley, 2007.

[36] L. L. Randeberg and L. O. Svaasand. Simulated color: A diagnostic tool for skin lesions like port-wine stain. *Lasers in Surgery: Advanced Characterization, Therapeutics, and Systems. Proceedings of* SPIE., 4244, 2001.

[37] F. A. Duck. *Physical properties of tissue: a comprehensive reference book*. Academic Pr, 1990.

[38] National Psoriasis Foundation. Statistics for psoriasis. `www.psoriasis.org/netcommunity/learn_statistics`, Ocrober 2009.

[39] J. M. Weinberg. *Treatment of Psoriasis*. Birkhauser, 2008.

[40] J. E. Gudjonsson and A. Johnston and H. Sigmundsdottir and H. Valdimarsson. Immunopathogenic Mechanisms in Psoriasis. *Clin Exp Immunol*, pages 135:1–8, 2004.

[41] B. Asher Louden, D. J. Pearce, W. Lang, and S. R. Feldman. A simplified psoriasis area severity index (SPASI) for rating psoriasis severity in clinic patients. *Dermatology Online Journal*, 10, 2004.

[42] T. Terui and H. Tagami. Mediators of inflammation involved in UVB erythema. *J Dermatol Sci*, pages 23:S1–S5, 2000.

[43] Y. Matsumura and H. N. Ananthaswamy. Toxic effects of ultraviolet radiation on the skin. *Toxicol Appl Pharmacol*, pages 195:298–308, 15 March 2004.

[44] D. Schmid, C. Schürch, and F. Zülli. Mycosporine-like amino acids from red algae protect against premature skin-aging. *Euro Cosmetics 09-06*.

[45] A.F. McKinlay and B.L. Diffey. A reference action spectrum for ultraviolet induced erythema in human skin. *CIE Journal*, pages 6:17–22, 1987.

[46] S. Madronich, R. L. McKenzie, L. O. Björn, and M. M. Caldwell. Environmental effects of ozone depletion. *Socioeconomic Data and Applications Center*, 1998.

[47] E. Hodak, A. B. Gottlieb, T. Segal, Y. Politi, L. Maron, J. Sulkes, and M. David. Climatotherapy at the dead sea is a remittive therapy for psoriasis: Combined effects on epidermal and immunologic activation. *J Am Acad Dermatol*, pages 49:451–7, 2002.

[48] J. A. Parrish and K. F. Jaenicke. Action spectrum for phototherapy of psoriasis. *J Invest Dermatol*, page 76:359–362, 1981.

[49] R. S. Stern and E. J. Lunder. Risk of squamous cell carcinoma and methoxsalen (psoralen) and UV-A radiation (PUVA): a meta-analysis. *Arch Dermatol*, pages 134:1582–5, 1998.

[50] Y. Yuehua, A. T. Khalaf, Z. Xiaoxiang, and W. Xinggang. Narrow-band ultraviolet B and conventional UVB phototherapy in psoriasis a randomised controlled trial. *Am J App Sci*, pages 5:905–908, 2008.

[51] E. Snellman, C. T. Jansen, J. Lauharanta, and P. Kolari. Solar ultraviolet (UV) radiation and UV doses received by patients during four-week climate therapy periods in the canary islands. *Photodermatol Photoimmunol Photomed*, pages 9:40–43, 1992.

[52] T. Gambichler, G. Moussa, N. S. Tomi, V. Paech, P. Altmeyer, and A. Kreuter. Reference limits for erythema-effective UV doses. *J Photochem Photobiol*, pages 82:1097–1102, 2006.

[53] Z. Even-Paz and D. Efron. Determination of solar ultraviolet dose in the dead sea treatment of psoriasis. *Isr Med Assoc J*, pages 5:87–88, 2003.

[54] T. Spott. *Characterization of Layered Tissue Structures with Diffusely Propagating Photon Density Waves*. Doctoral thesis NTNU, 1999.

[55] T. Spott and L. O. Svaasand. Collimated light sources in the diffusion approximation. *Appl. Opt.*, 39:6453–6465, 2000.

[56] A. Ishimaru. Theory and application of wave propagation and scattering in random media. *Proceedings of the* IEEE, 65:1030–1057, 1977.

[57] R. C. Haskell, L. O. Svaasand, T. Tsay, T. Feng, M. S. McAdams, and B. J. Tromberg. Boundary conditions for the diffusion equation in radiative transfer. *J. Opt. Am. A*, 11:2727–2741, 1994.

[58] L. O. Svaasand, L. T. Norvang, E. J. Fiskerstrand, E. K. S. Stopps, M. W. Berns, and J. S. Nelson. Tissue parameters determining the visual appearance of normal skin and port-wine stains. *Lasers in Medical Science*, 10:55–65, 1995.

[59] R. M. Pope and E. S. Fry. Absorption spectrum (380-700 nm) of pure water. II. integrating cavity measurements. *Appl. Opt.*, 36:8710–8723, 1997.

[60] J. W. Feather, M. Hajizadeh-Saffar, G.Leslie, and J. B. Dawson. A portable scanning reflectance spectrophotometer using visible wavelengths for the rapid measurement of skin pigments. *Physics in Medicine and Biology*, 34:807–820, 1989.

[61] L. L. Randeberg, O. A. Haugen, R. Haaverstad, and L. O. Svaasand. A novel approach to age determination of traumatic injuries by reflectance spectroscopy. *Laser Surg Med*, 38:277–289, 2006.

[62] L. L. Randeberg, E. B. Roll, L. T. N. Nilsen, T. Christensen, and L. O. Svaasand. In vivo spectroscopy of jaundiced newborn skin reveals more than a bilirubin index. *Acta Pediatrica*, 94:94:65–71, 2005.

[63] B. Riordan, S. Sprigle, and M. Linden. Testing the validity of erythema detection algorithms. *J Rehab Res Dev*, 38:13 – 22, 2001.

[64] L. V. Wang and H. Iwu. *Biomedical Optics, Principles and Imaging*. Wiley, 2007.

[65] R. Zhang, W. Verkruysse, B. Choi, J. A. Viator, B. Jung, L. O. Svaasand, G. Aguilar, and J. S. Nelson. Determination of human skin optical properties from spectrophotometric measurements based on optimization by genetic algorithms. *Journal of Biomedical Optics*, 10:024030, 2005.